Earth's Future

RESEARCH ARTICLE
10.1029/2019EF001210

Observed Impacts of Anthropogenic Climate Change on Wildfire in California

A. Park Williams[1], John T. Abatzoglou[2], Alexander Gershunov[3], Janin Guzman-Morales[3], Daniel A. Bishop[1,4], Jennifer K. Balch[5], and Dennis P. Lettenmaier[6]

[1]Lamont-Doherty Earth Observatory, Columbia University, Palisades, NY, USA, [2]Department of Geography, University of Idaho, Moscow, ID, USA, [3]Scripps Institution of Oceanography, University of California, San Diego, La Jolla, CA, USA, [4]Department of Earth and Environmental Sciences, Columbia University, New York, NY, USA, [5]Earth Lab/CIRES & Department of Geography, University of Colorado Boulder, Boulder, CO, USA, [6]Department of Geography, University of California, Los Angeles, CA, USA

Key Points:
- Annual burned area in California increased fivefold during 1972–2018, mainly due to summer forest fire
- Anthropogenic warming very likely increased summer forest fire by drying fuels; this trend is likely to continue
- Large fall fires are likely to become increasingly frequent with continued warming and possibly gradual declines in fall precipitation

Supporting Information:
- Supporting Information S1

Correspondence to:
A. P. Williams,
williams@ldeo.columbia.edu

Citation:
Williams, A. P., Abatzoglou, J. T., Gershunov, A., Guzman-Morales, J., Bishop, D. A., Balch, J. K., & Lettenmaier, D. P. (2019). Observed impacts of anthropogenic climate change on wildfire in California. *Earth's Future*, *7*, 892–910. https://doi.org/10.1029/2019EF001210

Received 14 MAR 2019
Accepted 28 JUN 2019
Accepted article online 15 JUN 2019
Published online 4 AUG 2019

Abstract Recent fire seasons have fueled intense speculation regarding the effect of anthropogenic climate change on wildfire in western North America and especially in California. During 1972–2018, California experienced a fivefold increase in annual burned area, mainly due to more than an eightfold increase in summer forest-fire extent. Increased summer forest-fire area very likely occurred due to increased atmospheric aridity caused by warming. Since the early 1970s, warm-season days warmed by approximately 1.4 °C as part of a centennial warming trend, significantly increasing the atmospheric vapor pressure deficit (VPD). These trends are consistent with anthropogenic trends simulated by climate models. The response of summer forest-fire area to VPD is exponential, meaning that warming has grown increasingly impactful. Robust interannual relationships between VPD and summer forest-fire area strongly suggest that nearly all of the increase in summer forest-fire area during 1972–2018 was driven by increased VPD. Climate change effects on summer wildfire were less evident in nonforested lands. In fall, wind events and delayed onset of winter precipitation are the dominant promoters of wildfire. While these variables did not change much over the past century, background warming and consequent fuel drying is increasingly enhancing the potential for large fall wildfires. Among the many processes important to California's diverse fire regimes, warming-driven fuel drying is the clearest link between anthropogenic climate change and increased California wildfire activity to date.

Plain Language Summary Since the early 1970s, California's annual wildfire extent increased fivefold, punctuated by extremely large and destructive wildfires in 2017 and 2018. This trend was mainly due to an eightfold increase in summertime forest-fire area and was very likely driven by drying of fuels promoted by human-induced warming. Warming effects were also apparent in the fall by enhancing the odds that fuels are dry when strong fall wind events occur. The ability of dry fuels to promote large fires is nonlinear, which has allowed warming to become increasingly impactful. Human-caused warming has already significantly enhanced wildfire activity in California, particularly in the forests of the Sierra Nevada and North Coast, and will likely continue to do so in the coming decades.

1. Introduction

In the western United States, annual area burned increased substantially in recent decades due to increased frequency and size of large wildfires (Abatzoglou & Williams, 2016; Balch et al., 2018; Dennison et al., 2014; Westerling, 2016). It is well established that this observed increase in wildfire activity was promoted in many areas by reduced fuel moisture due to warming-induced increases in evaporative demand, reduced snowpack, and reduced warm-season precipitation frequency (Abatzoglou & Williams, 2016; Holden et al., 2018; Kitzberger et al., 2017; Westerling, 2016). These recent climate trends are broadly consistent with those expected from anthropogenic climate change (Abatzoglou & Williams, 2016), but anthropogenic climate effects on wildfire can vary greatly across space and time due to confounding factors such as natural climate variations, land and fire management practices, ignitions from humans, spatial diversity in vegetation type, and the complex ways in which these processes interact (Williams & Abatzoglou, 2016). Therefore, location-

specific adaptation responses to wildfire require understanding how climate affects wildfire locally, how the key climate variables have changed over the past several decades, and whether these climate changes are likely to continue.

Perhaps nowhere on Earth has received more attention regarding recent wildfire trends and their causes than California. One reason for the attention is that increases in statewide burned area over the last several decades were dramatically punctuated in 2017 and 2018 by particularly extreme wildfire activity with substantial loss of life and property. In 2017, modern state records were set for the largest individual wildfire (Thomas Fire: 114,078 ha) and the most structures destroyed by an individual wildfire (Tubbs Fire: 5,636 structures), which led to 22 fatalities (CalFire, 2018). The total area burned in 2017 was also nearly a state record at the time (505,293 ha), behind 2007. In 2018, state records were set for total area burned (676,312 ha), largest individual wildfire (Mendocino Complex Fire: 185,800 ha), and most destructive wildfire (Camp Fire: 18,804 structures destroyed, 85 fatalities). In these 2 years, California spent over $1.5 billion on fire suppression, far more than any previous 2-year period (CalFire, 2018).

California is a particularly difficult place to disentangle the drivers of changing wildfire activity. California's climate, vegetation cover, and human settlement patterns are highly diverse, causing the influences of these factors on fire activity to be spatially heterogeneous and complex (Jin et al., 2014; Jin et al., 2015; Keeley & Syphard, 2017; Swetnam & Baisan, 2003; Westerling & Bryant, 2008). Humans dominate the wildfire regime across much of the state by altering land cover (Sleeter et al., 2011; Syphard et al., 2018), supplying the vast majority of ignitions (Balch et al., 2017; Nagy et al., 2018), and attempting to suppress essentially all fires. Fire suppression over the past century allowed for artificial buildup of fuels in many regions that historically experienced frequent low-intensity fires, reducing fuel limitation as a constraint on fire activity and putting many areas into a so-called fire deficit (Higuera et al., 2015; Marlon et al., 2012; Minnich et al., 1995; Parks et al., 2015). Even under constant climate conditions, changes in California's fire activity over the past century would be expected as populations increased and cities expanded into surrounding wildlands (Radeloff et al., 2018), fire suppression strategies evolved (Stephens & Ruth, 2005), and frequency and type of human-ignited wildfires changed (Balch et al., 2017; Keeley & Syphard, 2018). Changes in these nonclimatic factors may also promote nonstationarity in fire-climate relationships, confounding efforts to isolate the influence of climate change on fire activity (Higuera et al., 2015; Hurteau et al., 2019; Littell, 2018; Mann et al., 2016; Marlon et al., 2012; Taylor et al., 2016).

The effect of climate on wildfire in California is highly seasonal and variable across vegetation gradients. In summer, when fires are most frequent in California, large burned areas are promoted by the cumulative drying effects of atmospheric aridity and precipitation deficits mainly in forest ecosystems where fuel availability is not a limiting factor (Abatzoglou & Kolden, 2013; Jin et al., 2014; Keeley & Syphard, 2016; Swetnam, 1993; Swetnam & Betancourt, 1998; Westerling et al., 2003; Williams et al., 2018). In fall, many of California's most destructive fires occur in coastal shrublands and are driven by often extreme offshore downslope wind events, where synoptic conditions advect dry air masses often originating from the continental interior high desert westward and southward across topographic barriers such as the Transverse, Peninsular, and Coastal Ranges (Conil & Hall, 2006; Guzman-Morales et al., 2016; Hughes & Hall, 2010; Moritz et al., 2010; Nauslar et al., 2018). The most widely studied offshore wind events, termed Santa Ana winds in southern California, increase in frequency in the fall and peak in winter (Abatzoglou et al., 2013; Raphael, 2003). Strong offshore winds with very low relative humidity can quickly dry fuels and spread large wildfires when they occur prior to the onset of the winter precipitation season in California's Mediterranean climate (Billmire et al., 2014; Keeley, 2004; Moritz et al., 2010; Westerling et al., 2004).

The effects of anthropogenic climate change on California's fire regimes are likely to be diverse and complex, varying by region and season (Liang et al., 2017; Pierce et al., 2018; Syphard et al., 2019; Westerling, 2018). Climate model projections of warming and increased atmospheric aridity in California are strong and robust across models (Pierce et al., 2013). It is well established that warming promotes wildfire throughout the western United States, particularly in forested regions, by enhancing atmospheric moisture demand and reducing summer soil moisture as snowpack declines (Abatzoglou & Williams, 2016; Westerling et al., 2006). By contrast, model projections of precipitation in California are highly uncertain but with a tendency toward increased precipitation annual totals, particularly in northern California during winter (Maloney et al.,

2013). However, many climate models have systematic biases in North Pacific storm tracks and tropical Pacific sea surface temperatures that should lead to strong skepticism regarding model simulations of future precipitation in California (Seager et al., 2019; Simpson et al., 2016). Climate models also project precipitation frequency declines in spring through fall that would partly offset winter increases, resulting in increased precipitation variability (AghaKouchak et al., 2018; Pierce et al., 2018; Polade et al., 2014; Polade et al., 2017; Swain et al., 2018). In fall, models project reduced frequency and intensity of Santa Ana wind events (Guzman-Morales & Gershunov, 2019; Hughes et al., 2011). However, concurrent warming and decreased fall precipitation may, to some degree, counteract the effects of reduced offshore winds on fall fire risk in southwestern California (Hughes et al., 2011; Pierce et al., 2018), possibly extending the fire season towards the winter peak of the downslope wind season (Guzman-Morales & Gershunov, 2019; Syphard et al., 2018).

While much has been published on projected changes in wildfire activity due to climate change (e.g., Barbero et al., 2015; Hurteau et al., 2019; Krawchuk & Moritz, 2012; Littell et al., 2018; Westerling, 2018; Westerling et al., 2011; Westerling & Bryant, 2008), less has been done to evaluate *observed* seasonal trends in fire-relevant climate variables and whether these trends are consistent with those expected to arise from anthropogenic climate change. Here we provide a comprehensive empirical assessment of the observed effects of climate variability and change on California wildfire by season, region, and land cover. We first use wildfire and climate data within California to evaluate trends in seasonal burned area by region during 1972–2018, resolve the distinct seasonal and regional influences of climate and weather factors, and assess the stationarity of the dominant fire-climate relationships over the past five decades. We then use climate model simulations to determine whether observed trends in the climate variables most pertinent to regional wildfire activity are consistent with expectations of anthropogenic climate change. A thorough and nuanced understanding of how, when, and where anthropogenic climate change has or has not affected wildfire in California over the past several decades is critical to guide sustainable societal decisions ranging from where to develop housing to how limited resources can be optimized for landscape management.

2. Methods

A list of the publicly available sources for all data sets used in the analysis is provided in supporting information Table S1.

2.1. Study Regions

Because of the diversity of vegetation types, climate, fire regimes, and human population density, we divided California into four regions: North Coast, Sierra Nevada, Central Coast, and South Coast (see maps in Figure 1). North Coast and Sierra Nevada are largely forested, while Central and South Coast consist largely of grass-oak savanna, chaparral, and urban area, with some forest areas at high elevations. While humans ignite the majority of wildfires statewide, lightning accounts for the majority of ignitions in North Coast and Sierra Nevada, particularly in summer (Balch et al., 2017). Summer is the season when most burned area occurs on average in all for study regions, but large and destructive fires can also occur in fall in all regions, particularly in South Coast where fall marks the peak in mean fire size and suppression cost (Jin et al., 2015; Keeley et al., 2009). Regional boundaries were defined by merging Bailey ecoregions at the section level (Text S1). Regionalization by ecoregion is common in studies of regional climate-fire relationships, with some studies parsing more finely (Littell et al., 2018) or more coarsely (Abatzoglou et al., 2017) than we do here. We exclude the agricultural Central Valley and desert areas where large wildfires are rare due to lack of fuels.

2.2. Wildfire History and Climate Data

We compiled a comprehensive record of 39,556 California wildfires during 1972–2018 within our four regions of interest by merging records from multiple government agencies. We excluded all fires smaller than 0.1 ha, as these fires are inconsistently reported and contribute negligibly to total regional burned area. We did not consider years prior to 1972 as this is when most of the multiagency records begin. There is high confidence in these historical records of burned area (Keeley & Syphard, 2018). Regional burned-area records were reproduced for forest and nonforest land cover types (e.g., Abatzoglou & Williams, 2016). See Text S2 for additional details about the wildfire data set.

To evaluate observed climate trends in the context of anthropogenic climate change, it is desirable to evaluate a period longer than the 1972–2018 wildfire record. The temporal extent of the climate records varies by variable and data product. Table S1 provides the temporal coverage of all data sets used. Monthly climate grids for 1895–2018 came from the National Oceanic and Atmospheric Administration's Climgrid data set for precipitation and temperature (Vose et al., 2014), PRISM for humidity (Daly et al., 2004), and a multiproduct data set compiled by Williams et al. (2017) for wind speed and solar radiation. See Text S3 for details. Daily meteorological grids from gridMET (Abatzoglou, 2013) were used to calculate two daily fire-potential indicators for 1979–2018: 1,000-hr fuel moisture (FM1000) and the Fosberg Fire Weather Index (FFWI). The FM1000 (Cohen & Deeming, 1985) is a water-balance variable that uses precipitation, temperature, and humidity to track moisture content in large-diameter dead fuels and exhibits significant relationships to fire activity (e.g., Abatzoglou & Kolden, 2013; Marlier et al., 2017). The FFWI is a proxy for fire potential and spread that is based on wind speed, humidity, and temperature with no memory of antecedent conditions (Fosberg, 1978) and has been linked to significant wind-driven fires in southern California (e.g., Barbero et al., 2014; Moritz et al., 2010). The FM1000 and FFWI records were extended to 1948 using the climate reanalysis dataset from the National Centers for Environmental Prediction and Atmospheric Research (NCEP-NCAR; Kalnay et al., 1996) and Climgrid. For FFWI, we commence our analyses in 1958 due to an unrealistic positive trend in 1948–1957 NCEP-NCAR 10-m wind speed that is likely an artifact of the widespread expansion of rawinsonde measurements during this period. See Text S4 for more details about these records. Daily weather-station precipitation totals for 1915–2018 come from the Global Historical Climatology Network version 3.25 (Menne et al., 2012) and were used to evaluate seasonal precipitation frequency and the onset of the winter precipitation season. Gap filling was performed using nearby stations and gridded daily records from PRISM and Livneh et al. (2013, 2015). See Text S5 for details. To represent the timing of onset of the winter precipitation season, we evaluate the number of days needed to reach 10% of the fall (October–December) long-term mean precipitation total. We also evaluate wet-day frequency in October–November, defined as days when precipitation $\geq$2.54 mm (Holden et al., 2018).

To evaluate observed and modeled trends in fire-promoting interannual precipitation volatility (wet years that grow fuels followed by dry years that dry fuels out), we examined the running 10-year frequency of "wet-dry events," which we define here (building off of Swain et al., 2018) as events in which a lowest 20% water-year (October–September) precipitation total follows a highest 20% precipitation total in at least one of the two preceding water years.

The simulated climate response to anthropogenic forcing was assessed using climate model simulations produced as part of the fifth phase of the Coupled Model Intercomparison Project (CMIP5; Taylor et al., 2012). The forcing scenarios considered were the Historical scenario for 1851–2005 and the 8.5 representative concentration pathway (RCP8.5) scenario for 2006–2100 (van Vuuren et al., 2011). The RCP8.5 represents a plausible upper-end emissions scenario, but projections over the next few decades are similar to those projected for the RCP4.5 emissions scenario, which more strongly departs from RCP8.5 in the second half of this century due to reduced anthropogenic greenhouse gas emissions (Pierce et al., 2018). See Table S2 for a list of all CMIP5 models considered for each variable.

2.3. Relationships Between Climate and Wildfire

We evaluate interannual relationships between climate and the logarithm of seasonal and annual burned area (log(burned area)) using linear regression and the Pearson correlation coefficient. We used the logarithms of burned area because burned area has an exponential distribution (e.g., Keeley & Syphard, 2017; Littell et al., 2009). Climate variables considered in the regression analyses were precipitation total, wet-day frequency, mean daily maximum temperature (Tmax), mean daily minimum temperature (Tmin), vapor pressure deficit (VPD), wind speed, solar radiation, the Penman-Monteith reference evapotranspiration (Monteith, 1965; Allen et al., 1998; Text S3), and FM1000. VPD is a measure of the aridity of the atmosphere, calculated as the difference between the saturation vapor pressure (dictated by temperature) and the actual vapor pressure (dictated by specific humidity; Text S3). Time series of precipitation total were converted to the standardized precipitation index (SPI) because raw precipitation totals often have a skewed nonnormal distribution.

The regression analyses were conducted at the regional and all-region scales and were repeated for forest and nonforest burned areas. Climate effects on wildfire vary among seasons. For example, precipitation can suppress wildfire during and immediately prior to the fire season by increasing fuel moisture but can have the opposite effect in the years prior to the wildfire year by promoting fuel growth in fuel-limited fire regimes (Swetnam & Betancourt, 1998). We therefore evaluated in a supplemental analysis the correlation between seasonal burned area records and each climate variable during the wildfire year as well as the 2 years prior, averaging each variable over a sliding window of 1–36 months. This supplemental analysis guided our decisions as to the ranges of months to consider when regressing burned-area records against records of climate data. For example, the period of optimal positive influence on antecedent precipitation is defined as the range of months within the 36-month period when SPI correlates most positively with the burned area record. To test for an independent relationship between a climate variable (Variable B) and burned area after relationships with another climate variable (Variable A) have been accounted for, we performed a partial regression analysis. Here time series of log(burned area) and Variable B were each regressed against Variable A. Residuals for log(burned area) and Variable B were calculated by subtracting away the linear relationships with Variable A. The two residual time series were then regressed against each other to assess the component of the relationship between burned area and Variable B that is independent of Variable A.

For fall, we evaluated how subseasonal climate conditions affect the daily probability of a large wildfire occurring (defined in each region as the largest 15% of fall wildfires to occur in that region during 1972–2017, as the record of 2018 wildfires was incomplete). Specifically, we used 3-day means of regionally averaged FM1000 and FFWI as logistic predictors of whether a fall day had at least one large fall wildfire.

We did not control for nonclimate effects on wildfire such as human effects on ignitions, fire suppression, or vegetation cover. Therefore, the climate-fire relationships that we identified have human impacts embedded within them (e.g., human effects on land cover may influence how wildfire responds to drought). When relevant, we evaluated the stability of fire-climate relationships during 1972–2018 by comparing regression statistics based on only data from 1792–1999 versus 2000–2018. Similar statistical relationships for both periods would strongly suggest that, while nonclimate factors may influence the fire-climate relationship in general, these factors (e.g., fuel accumulation due to wildfire suppression) did not cause a change in the fire-climate relationship during the study period.

2.4. Trend Analysis

We assessed observed and simulated trends in climate records longer than 60 years using a 50-year low-pass 10-point Butterworth filter because anthropogenic climate trends are not linear (e.g., Williams et al., 2015). Trend magnitude is assessed as the final low-pass filtered value minus the first. For time series of burned area during 1972–2018, we assessed trend slope for log(burned area) using the nonparametric Theil-Sen estimator, which is more robust to outliers than the least-squares method (Sen, 1968). For trend significance, we considered (conservatively) all trends to be linear functions of time (not low-pass filtered), with significance assessed using the nonparametric Spearman's rho and Kendall's tau tests. We only interpreted trends as statistically significant if both tests passed at the 95% confidence level ($p < 0.05$). We interpreted CMIP5 ensemble-mean trends as the forced climate response to anthropogenic emissions. To assess significance of anthropogenic trends, we superimposed observed high-frequency climate variability (50-year high-pass filter) onto the CMIP5 ensemble-mean 50-year low-pass filtered trend and then evaluated significance as described above.

3. Results and Discussion

3.1. Historical Trends in Burned Area

Annual burned area across our study regions in California increased significantly ($p < 0.01$) by 405% during 1972–2018 (Figure 1a). In 2017 and 2018, the total area burned ranked third and first largest during our study period, respectively. This statewide increase was driven by significant increases in North Coast and Sierra Nevada (Figures 1b and 1c). In these regions, annual burned areas increased by 630% and 618%, respectively. Annual burned area did not change significantly in Central and South Coast (Figures 1c and 1d).

The increases in California burned area occurred mainly in summer (May–September), the season when burned areas are largest overall (Figures 1 and S1). All-region summer burned areas in 2017 and 2018

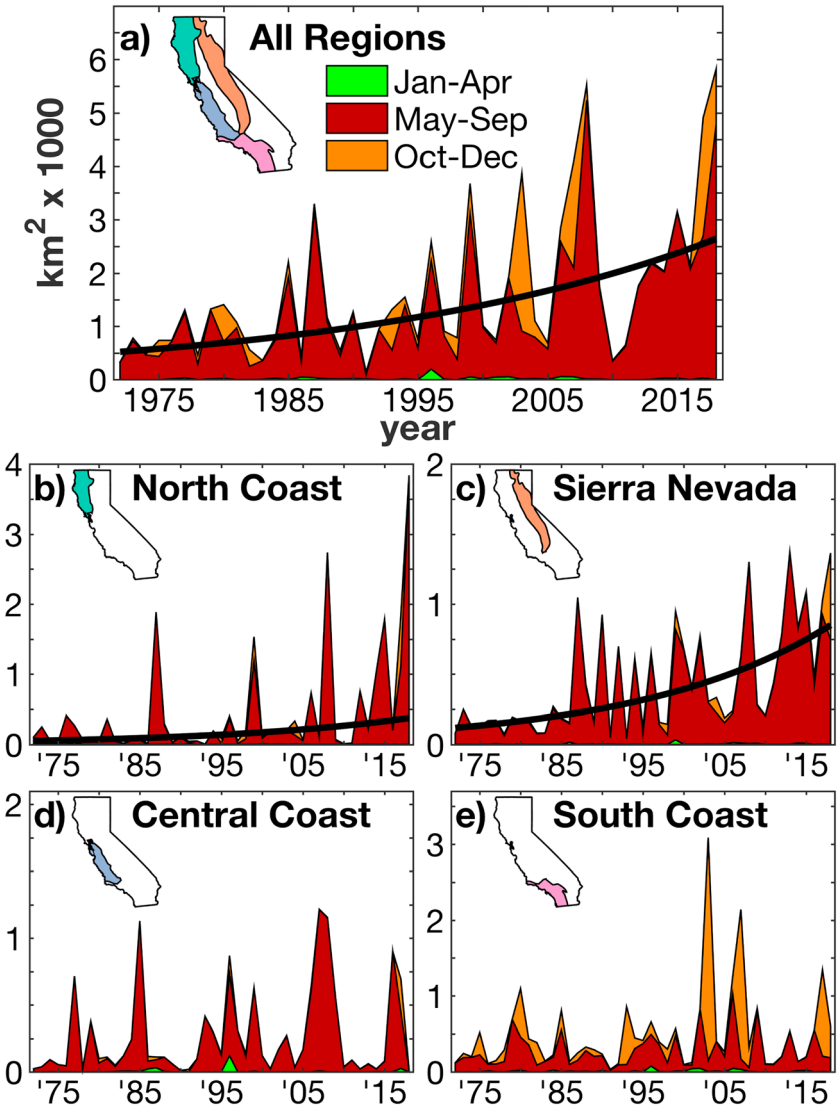

Figure 1. Seasonal and annual burned areas in California for 1972–2018. (a) Total burned area in the four regions of focus: (b) North Coast, (c) Sierra Nevada, (d) Central Coast, and (e) South Coast. Annual burned area is decomposed into that which occurred in January–April (green), May–September (red), and October–December (orange). Significant ($p < 0.05$) trends are shown as bold black curves.

ranked sixth and second largest, respectively. The summer increases in burned area were most significant (+766%) in forested areas, and these increases were dominated by North Coast and Sierra Nevada, where approximately three quarters of California's forest-fire area occurred during 1972–2018 (Figure S2 vs. Figure S3). During 1972–2018, the proportion of summer burned area occurring in forest increased significantly ($p < 0.01$) from a mean of 51% in the 1970s to 71% in the 2010s.

Trends in fall burned area since 1972 generally do not pass significance tests (Figure S1), but fall burned area in 2017 and/or 2018 was much higher than average in all four regions (Figure S1). The general lack of significant trends in fall is partly due to high interannual variability, driven by large wildfires in relatively few years. Despite lack of significant trends, large fall wildfires in North Coast and Sierra Nevada (≥85th percentile among fall wildfires in each region) were 3.8 and 2.3 times more common, respectively, in the second half of the record (1996–2017) than in the first (1972–1995). As was the case for summer, increases in the occurrence of large fall wildfires were observed in North Coast and Sierra Nevada but not for Central or South Coast.

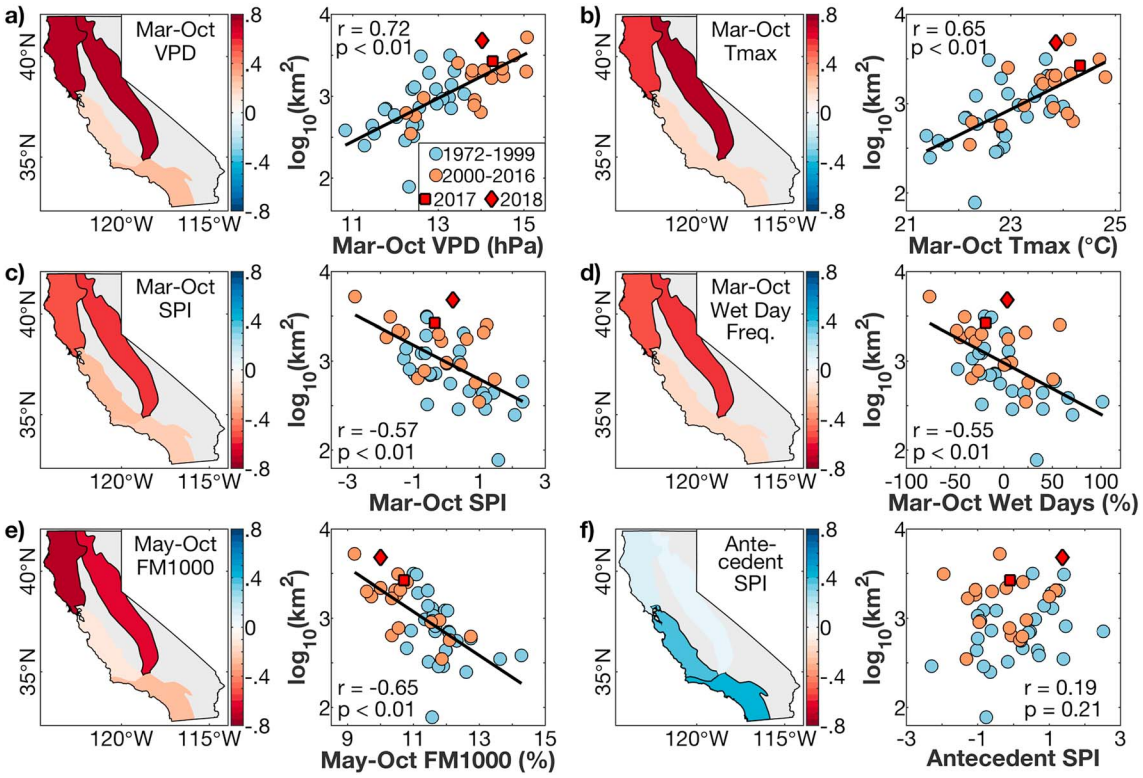

Figure 2. Correlation between summer (May–September) burned area and climate: 1972–2018. Maps: Regional correlations between the logarithm of summer burned area and mean seasonal climate (outline around region: $p < 0.05$). Scatterplots represent the full study domain. Climate variables in (a–f): vapor-pressure deficit (VPD), daily maximum temperature (Tmax), standardized precipitation index (SPI), Wet Day Frequency (frequency of days with precipitation total ≥2.54 mm), 1,000-hr dead fuel moisture (FM1000), and SPI from March of 2 years prior to the fire year through October of the year prior to the fire year (Antecedent SPI). Colors in scatter plots correspond to the legend in (a).

3.2. Climate Controls on Wildfire

3.2.1. Summer Wildfire

Figure 2 shows that among the climate variables considered, all-region summer burned area correlated most strongly with warm-season (March–October) VPD ($r = 0.72$, $p < 0.01$; Figure 2a). VPD is most strongly influenced by Tmax due to the exponential Clausius-Clapeyron effect of temperature on saturation vapor pressure, explaining why summer burned area correlates more strongly with warm-season mean Tmax ($r = 0.65$, $p < 0.01$; Figure 2b) than with the other components of VPD: Tmin ($r = 0.46$, $p < 0.01$) and vapor pressure ($r = -0.36$, $p < 0.05$).

On a regional basis, the fire-promoting effects of fuel aridity (high VPD, precipitation deficit, and low fuel moisture) were more strongly correlated with burned area in the wetter and more heavily forested North Coast and Sierra Nevada than in the drier and less forested Central or South Coast (Figures 2a–2d and S4). In fact, forest areas were mostly responsible for the strong correlation between fuel aridity variables and burned area (Figures S5 and S6); correlation between summer all-region burned area and warm-season VPD was 0.79 ($p < 0.01$) in forest areas but only 0.35 ($p < 0.05$) in nonforest areas (Figures S5c and S5d). This result is consistent with the tendency for interannual variability in regional burned area to be more sensitive to variations in fuel aridity in more heavily vegetated zones where fuel abundance is less limiting (Abatzoglou et al., 2018; Littell et al., 2018; McKenzie & Littell, 2016).

Consistent with previous findings (e.g., Keeley & Syphard, 2017), the correlation between burned area and climate was relatively weak in Central and South Coast (Figure 2). This is likely partly because fire-climate relationships in these regions are strongly manipulated by humans via ignitions, suppression, and land cover change (Balch et al., 2017; Sleeter et al., 2011; Syphard et al., 2017). In addition, aboveground biomass is generally lower in these regions due to warmer and drier conditions, causing fuel availability to often limit fire spread in grasslands and potentially shrublands with nonnative grasses (Keeley, 2004). Similar to

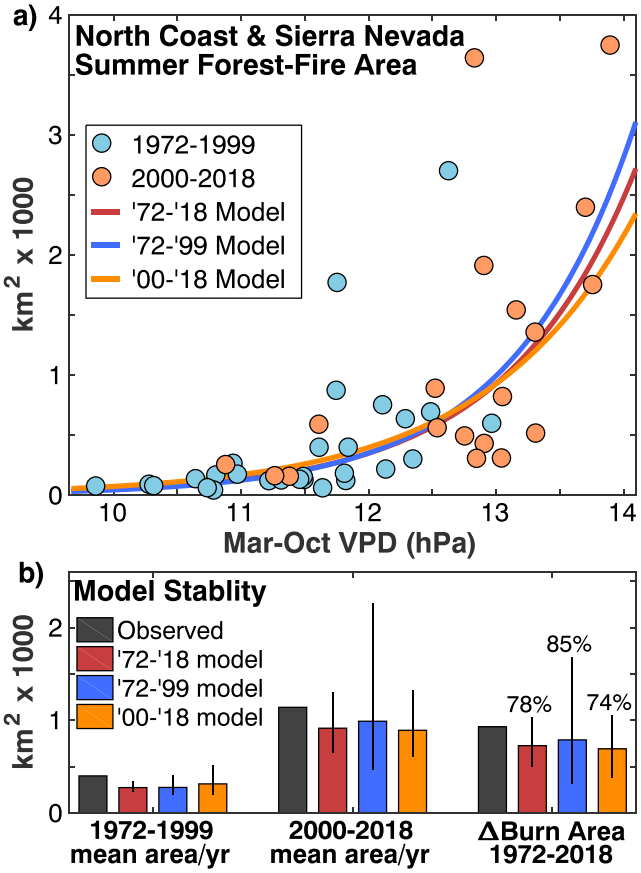

Figure 3. Response of forest-fire area to atmospheric aridity. (a) Scatter plot of (*y* axis) annual summer (May–September) forest-fire area versus (*x* axis) mean warm-season (March–October) vapor-pressure deficit (VPD) in North Coast and Sierra Nevada. Curves represent regression fits to (maroon) the full 1972–2018 data set, (blue) 1972–1999, and (orange) 2000–2018 based on the least-squares linear regression between log(burned area) and VPD. (b) Temporal stability of the relationship shown in (a). Each curve in (a) was used to estimate mean summer forest fire area in 1972–1999 and 2000–2018 as well as the change in mean summer forest fire area due to linear increase in 1972–2018 warm-season VPD. Whiskers: 95% confidence intervals. Black bars: observations. Percentages above the bars on the right indicate the percent of the observed increase in 1972–2018 forest-fire area that is accounted for by the observed increase in warm-season VPD.

relationships in traditionally fuel-limited fire regimes, burned area in South and Central Coast was positively and significantly correlated with antecedent precipitation over the preceding 2 years, which promotes fine-fuel accumulation (Bradstock, 2010; Batllori et al., 2013; Abatzoglou et al., 2018; Littell et al., 2018; Figures 2f, S4, S5, and S7). After removing the positive relationship with SPI via linear regression (identifying the range of months when SPI is most positively correlated with summer nonforest burned area in each region), burned area is secondarily promoted by current-year moisture deficit, which promotes fuel drying (Figure S7). This highlights the likelihood that nonforest wildfire is promoted by large interannual swings in precipitation total, from wet conditions that drive accumulation of grasses to dry conditions that promote desiccation of fuels. Similarly, while the fire-promoting effect of VPD is far weaker in nonforest than in forest, warm-season VPD correlated positively and significantly (r = 0.29–0.50, $p < 0.05$) with residual time series of summer nonforest burned area in North, Central, and South Coast after removal of antecedent precipitation effects (Figure S8). Warm-season aridity and drought therefore appear to be secondarily but still weakly influential on summer wildfire in many nonforest parts of California. Importantly, nonforested landscapes in California are highly diverse, and the broad patterns described above do not apply everywhere. In many chaparral ecosystems, for example, vegetation is dense and fuel is generally not limiting (Keeley & Fotheringham, 2001), but large wildfires that burn across multiple chaparral communities are nonetheless likely to be promoted when grasses are abundant to provide connectivity.

Finally, in areas where wildfire is promoted by dry conditions, burned area tends to correlate more strongly with atmospheric aridity (e.g., VPD) than with precipitation or more integrative moisture-balance metrics (Figure 2). This was observed previously across broader portions of the western United States (e.g., Abatzoglou & Williams, 2016; Williams et al., 2015) and may be partly representative of the importance of fine dead fuels to fire spread, which can quickly equilibrate with atmospheric moisture content (Matthews, 2014). However, correlative analyses with a single variable may artificially confound or inflate its importance due to covariance with other variables or factors (Holden et al., 2018; Williams, Seager, Macalady, et al., 2015). For example, VPD is negatively related to precipitation (cloud shade and soil moisture negatively force VPD), so the effect of one variable is entrained in the correlation between burned area and the other variable. Importantly, the positive correlation between summer burned area and March–October VPD remained strong and significant (0.64–0.67, $p < 0.01$) in North Coast and Sierra Nevada forests after accounting for the co-occurring negative effects of precipitation on VPD and burned area (Figure S9). Accounting for precipitation does not change the result that increases in summer burned forest area during our study period corresponded to increases in warm-season VPD, as 2000–2018 burned area and VPD anomalies both remain strongly positive after covariability with precipitation has been removed. These results support VPD as a leading driver of the observed trends in forest-fire area in California during 1972–2018.

The scatter plots in Figure 2 strongly suggest that aridification was the primary driver of the observed increase in California burned area during 1972–2018, as indicated by the visible offsets (particularly in Figure 2a) between the cooler and less arid pre-2000s period and the warmer and more arid 2000s period. Further, the effect of aridity on burned area (which is strongest in forest) is exponential (as implied by the log scale of the *y* axes). This is clearly demonstrated in Figure 3a, which shows the strong, nonlinear response of summer forest-fire area to warm-season VPD in the heavily forested North Coast and Sierra Nevada. Because of the exponential nature of this response, each incremental increase in VPD leads to a larger

burned-area response than the previous. Based on the regression shown in Figure 3a, the linear increase in warm-season VPD during 1972–2018 (+1.3 standard deviations) accounted for approximately 78% of the observed increase in summer forest-fire area (Figure 3b). Importantly, the strong relationship between warm-season VPD and summer forest-fire area was stable during the study period, as indicated by statistically indistinguishable regression models regardless of whether the regression was built on the full study period, 1972–1999, or 2000–2018 (Figures 3 and S10). The temporal stability of the relationship between forest-fire area and VPD indicates that the importance of VPD to forest-fire area was not amplified or overtaken by another climatic or nonclimatic variable during the study period.

The above results strongly suggest that the observed increase in California summer burned area during 1972–2018 (which mainly occurred in northern California forests) was mainly due to increased VPD and not concurrent changes in nonclimate factors such as forest management, fire suppression practices, or human ignitions. This is not to say that nonclimate factors were negligible in dictating modern annual burned areas. To the contrary, human ignitions greatly enhance the number of wildfires relative to that expected in their absence (Balch et al., 2017), and increased fuel density due to fire suppression (and warming/wetting trends in the high Sierra) may have enhanced the mean state of modern-day forest-fire extent, severity, and sensitivity to aridity (Dolanc et al., 2013; Harris & Taylor, 2015; Minnich et al., 1995; Swetnam & Baisan, 1996). However, while effects of human activities are evident in multicentury assessments of fire activity (e.g., Klimaszewski-Patterson et al., 2018; Marlon et al., 2012; Taylor et al., 2016), changes in background conditions such as fuel abundance *during* our short study period do not appear responsible for the observed increase in summer forest-fire extent during 1972–2018.

3.2.2. Fall Wildfire

Interannual correlation between fall total burned area and climate is weak because fall burned areas are dominated by a small number of years. On an intraseasonal basis, however, the daily probability of a large fall wildfire occurring in a given region (*Pfire*) was significantly higher during 3-day periods with low fuel moisture and high wind-driven fire danger (Figures 4 and S11). For each region, both independent variables contribute significantly to prediction skill (Table S3 for model coefficients and significance values). For all regions, mean *Pfire* on days with at least one large fall wildfire exceeded twice that of days with no large fall wildfire. This result was sustained for out-of-sample estimates of *Pfire*, where each year's *Pfire* values were estimated using a prediction model built from all other years. In 2017 and 2018, nearly all wildfires qualifying as among the 10 largest fall wildfires since 1972, including the particularly destructive Camp, Thomas, and North Bay fires, occurred when *Pfire* was near or at record daily high levels (Figure 4). Importantly, many of the large wildfires that occur under dry conditions during fall are in nonforest landscapes where *summer* burned area does not appear to be strongly promoted by drought. In contrast to summer, when many nonforest areas are consistently hot and dry, an aridity limitation on nonforest wildfire may emerge during fall due to lower temperatures and onset of the precipitation during that season.

3.3. Climate Trends Important to Wildfire

3.3.1. Summer

The largest wildfire-relevant climate trend in summer was a significant warming-driven increase in VPD (Figures 5a and 5b). During 1896–2018, March–October Tmax averaged across the four California study regions increased by 1.81 °C, with a corresponding increase in VPD of 1.59 hPa (+13%). Warm-season VPD in 2017 and 2018 was, respectively, sixth and ninth highest since at least 1896. The observed centennial trends in Tmax and VPD are consistent with trends simulated by climate models as part of the CMIP5 experiments, supporting the interpretation that observed increases in California warm-season temperature and VPD have been largely or entirely driven by anthropogenic forcing. These results are consistent across the four regions, though in South Coast, observed increases in Tmax and VPD have outpaced CMIP5 increases (Figures S12–S15). Discrepancies between observed and simulated (climate model) trends in South Coast may be due to a range of factors including natural multidecade climate variability (Lehner et al., 2018), urbanization effects (Williams et al., 2015; Williams et al., 2018), and inability of global climate models to capture fine-scale cloud and circulation features (Sun et al., 2015; Walton et al., 2015).

Unlike temperature and VPD, there was no significant long-term trend in all-region mean precipitation (SPI) during March–October or November–February (Figures 5c and 5d). This was also consistent with the CMIP5 simulated trends. The CMIP5 ensemble-mean trends in precipitation are slightly negative for

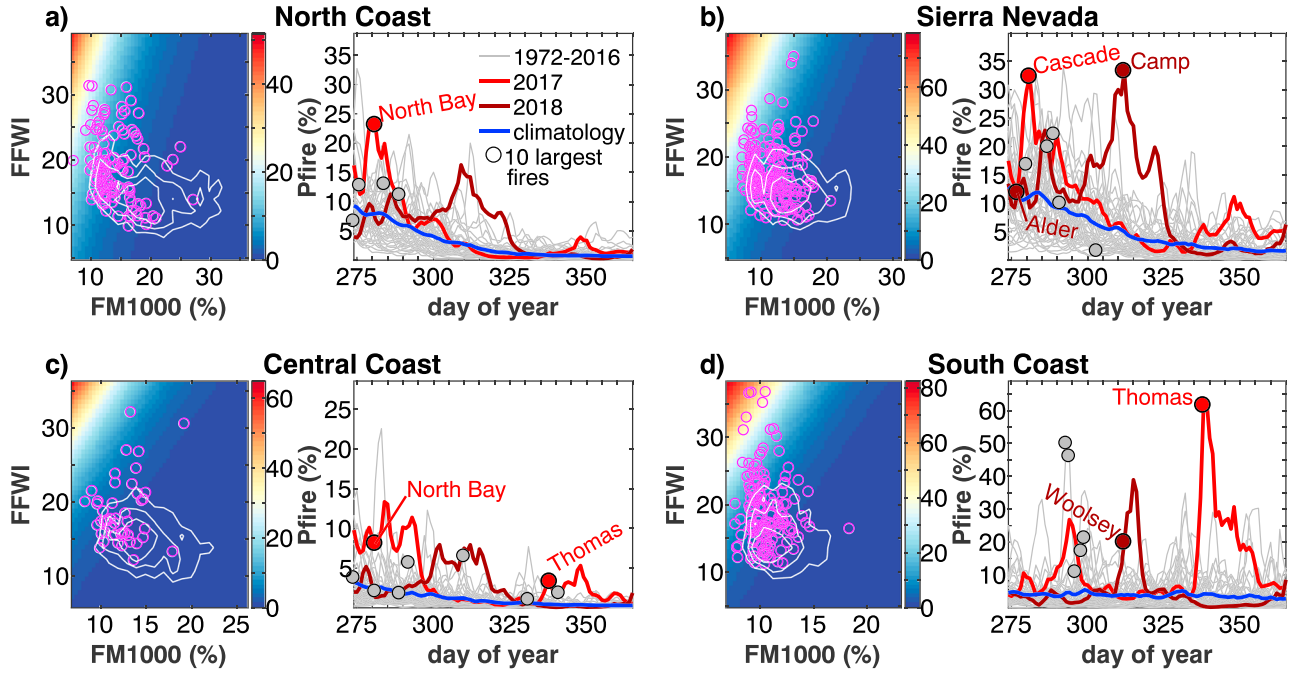

Figure 4. Daily regional probability of ≥1 large fall wildfire (Pfire) as a function of Fosberg Fire Weather Index (FFWI) and 1,000-hr dead fuel moisture (FM1000). Large wildfires: largest 15% of fall wildfires ≥0.1 ha in each region during 1972–2017. Background colors in the plots on the left for each region show the result of a bivariate logistic regression model that estimates *Pfire*. (magenta circles) Days with large fall wildfires. White contours bound 75%, 50%, and 25% of days without large fall wildfire. Time series plots on the right show daily *Pfire* for all fall seasons during 1972–2018 based on observed FFWI and FM1000. FM1000 and FFWI values represent 3-day means (Day 0 through Day +2) because large fires grow over multiple days. Names of the large fires in 2017 and 2018 are provided. "North Bay" represents the cluster of fires that occurred in October 2017 in the northern Bay Area. Fires that appear in multiple time series burned large areas in multiple regions.

March–October and slightly positive for November-February during 1896–2018, but the magnitudes of these trends are small relative to interannual variability. For March–October, just 3 of 42 climate models indicate significant negative trends (0 significant positive trends). For November–February, just 1 of 42 climate models indicates a significant positive trend (0 significant negative trends). These all-region results are generally consistent at the regional level with the exception of March–October SPI in South Coast, where warm-season precipitation declined significantly (>1.5 σ) during 1896–2018 (Figures S12–S15). The observed warm-season precipitation reduction in South Coast was larger than that represented by the CMIP5 multimodel mean (Figure S15c).

The black line in Figure 5e shows that May–October FM1000 significantly ($p < 0.05$) decreased over the past 70 years largely due to declines over the past four decades. May–October FM1000 ranked fifth and fifteenth lowest on record (1948–2018) in 2017 and 2018, respectively. The blue time series shows FM1000 after linear trends in temperature and relative humidity since 1948 were removed. The lack of trend in the blue line relative to the observed FM1000 trend indicates that warming (Figures 5a and 5b) drove the significant decline in May–October FM1000. This result was consistent for North Coast, Sierra Nevada, and Central Coast (Figures S12–S15). In South Coast, warming did not significantly reduce May–October FM1000 during 1948–2018 because of large decadal variations in precipitation (Figure S15). Much of South Coast experienced significantly reduced summer cloud shading over the past several decades, likely reducing summer fuel moisture, but this effect is not well represented in gridded climate data sets (Williams et al., 2018). Additionally, warming further reduces warm-season fuel moisture in snow-dominated areas by reducing snowpack and extending the snow-free period (Evan, 2019; Kitzberger et al., 2017; Westerling, 2016; Westerling et al., 2006). Mote et al. (2018) showed that spring snowpack declined throughout the Sierra Nevada during 1955–2016 and attributed much of this change to warming, consistent with previous hydroclimate modeling results (Barnett et al., 2008).

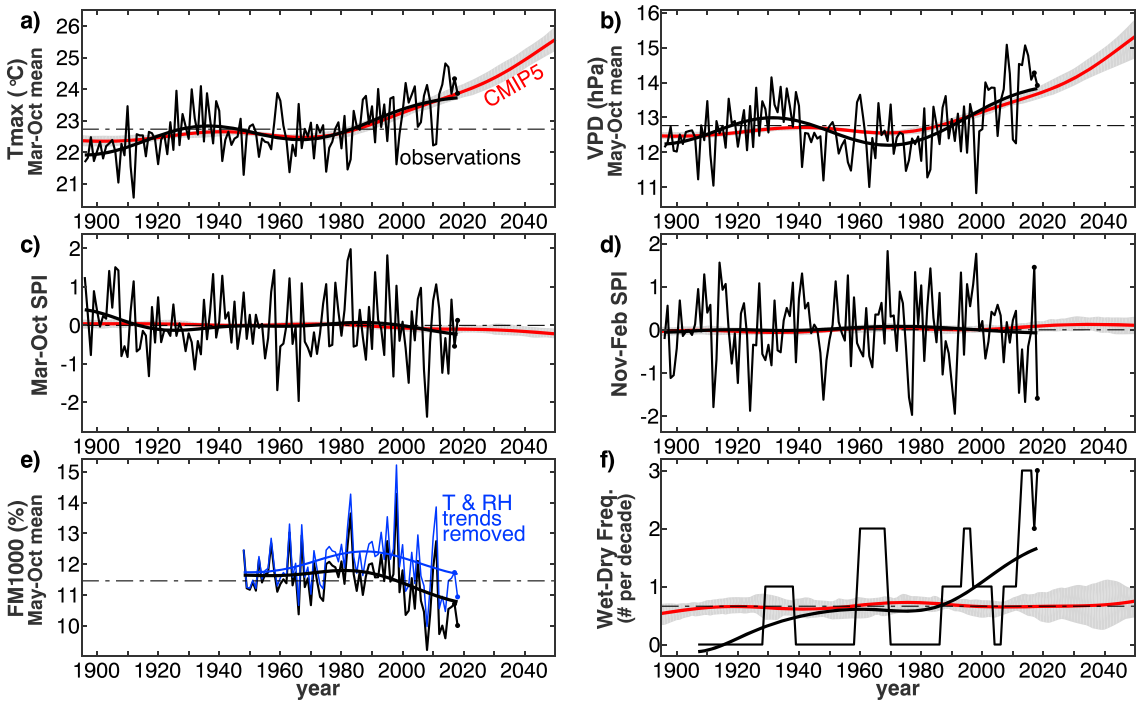

Figure 5. Mean all-region trends in climate variables important to summer wildfire. (a–c) March–October mean daily maximum temperature (Tmax), vapor-pressure deficit (VPD), and standardized precipitation index (SPI), respectively. (d) November–February SPI. (e) May–October mean 1,000-hr dead fuel moisture (FM1000). (f) Number of "wet-dry" events per decade, when at least one of the 2 water years (WYs) preceding a dry WY was wet (WY: October-September). Wet and dry WYs: precipitation total greater and lower than the 80th and 20th percentiles of a 1921–2000 baseline, respectively. Black record: observations (2017–2018 indicated with black dots) and (bold curve) 50-year low-pass filter. Blue record in (e): FM1000 after removal of linear temperature (T) and relative humidity (RH) trends from 1948–2018. Red curve: fifth phase of the Coupled Model Intercomparison Project (CMIP5) ensemble-mean 50-year low-pass filtered time series (gray areas bound interquartiles of 50-year low-pass filtered time series among climate models). Horizontal black lines: observed mean. See Figures S12–S15 for trends in the individual regions.

Biomass abundance appears to regulate how drought and aridity affect summer burned area in nonforest landscapes, particularly in Central and South Coast. In these regions, fire risk may be promoted by wet-dry events (see Methods), when increased fine-fuel biomass due to high precipitation total in one year dries out due low precipitation in a subsequent year. The observed frequency of wet-dry events increased over the past century (Figure 5f), and this increase was at the margin of the $p < 0.05$ one-tailed significance level based on 10,000 repetitions with randomized precipitation records. The observed centennial increase in wet-dry event frequency occurred mainly as a result of an increase in interannual variability in total annual precipitation (Figure S16). Climate models do project increased interannual variability of California precipitation at a range of temporal scales (Berg & Hall, 2015; Pendergrass et al., 2017; Polade et al., 2014; Polade et al., 2017; Swain et al., 2018), but the multi-model mean suggests no clear anthropogenic promotion of wet-dry events as of 2018 (Figures 5f and S16).

It has been projected that warming should promote increased lightning frequency across the Unites States (Romps et al., 2014), but we do not evaluate lightning effects here. Increased lightning would likely promote increased summer wildfire frequency where it is not accompanied with wetting precipitation, but the effect on area burned would likely be small, as the relationship between annual area burned and lightning frequency is weak in North Coast and Sierra Nevada, where California's lightning frequency is the highest (Abatzoglou et al., 2016).

3.3.2. Fall

The connection between fall wildfire and anthropogenic climate change is less clear than in summer. Large fall wildfires generally require a strong dry wind event (e.g., Santa Ana winds) to intersect with dry fuels and ignitions. Fuels in fall can remain dry enough to burn until commencement of the winter precipitation season and lower temperatures, which generally occurs in early to mid-fall. Therefore, a change in the onset of

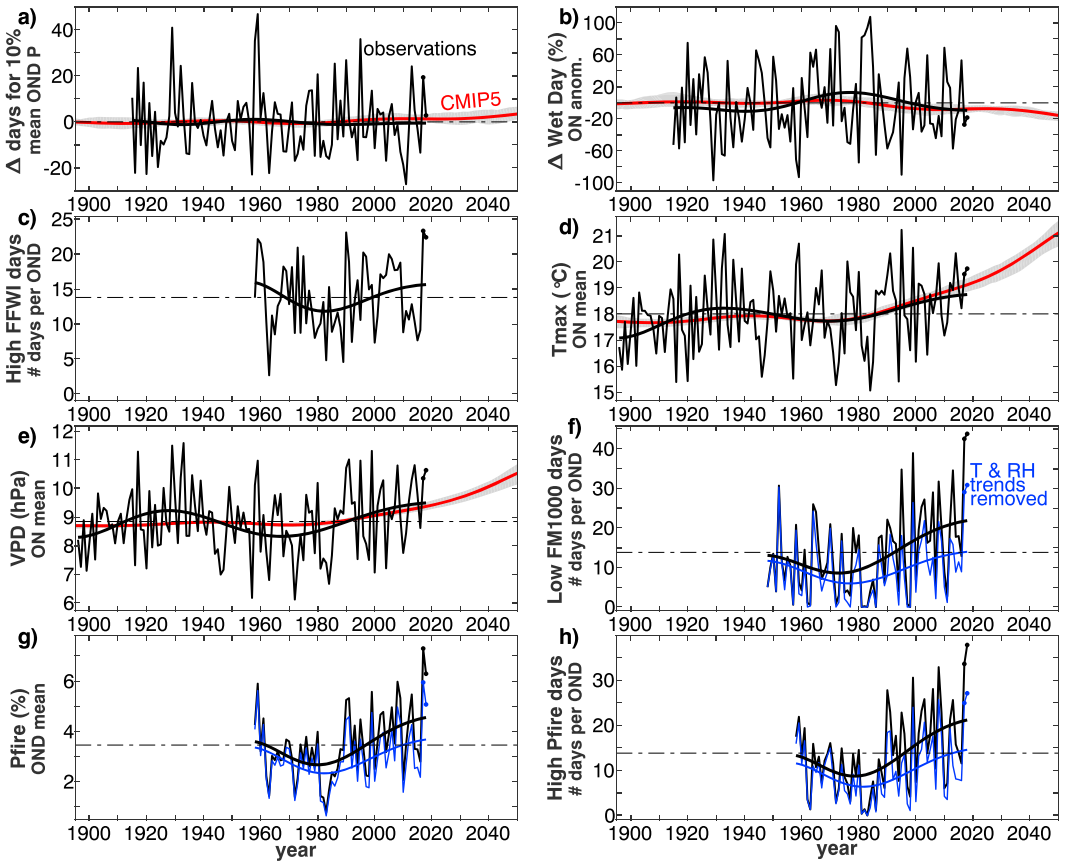

Figure 6. Mean all-region trends in climate variables important to fall wildfire. (a,b) Anomalies in the (a) number of days needed to reach 10% of mean October–December (OND) precipitation and (b) percent of OND wet days (precipitation total ≥2.54 mm). (c) Number of OND days with high (≥85th percentile) Fosberg Fire Weather Index (FFWI). (d,e) October–November (ON) mean daily maximum temperature (Tmax) and vapor-pressure deficit (VPD), respectively. (f) Number of OND days with low (≤15th percentile) 1,000-hr dead fuel moisture (FM1000). (g) OND all-region mean daily probability of a large (top 15%) fall wildfire (*Pfire*), calculated from FM1000 and FFWI (Figure 4). (h) Number of OND days with high (>85th percentile) Pfire. Black time series: observations (black dots: 2017–2018) and (bold curve) 50-year low-pass filter. Blue: observations after removal of linear temperature (T) and relative humidity (RH) trends from 1948–2018. Red: fifth phase of the Coupled Model Intercomparison Project (CMIP5) ensemble-mean 50-year low-pass filtered time series (gray areas bound interquartiles of 50-year low-pass filtered time series among climate models). Horizontal black lines: observed mean. See Figures S17–S20 for trends in the individual regions.

the winter precipitation season or a change in the frequency or intensity of dry wind events in fall would likely affect fall wildfire activity.

Figures 6a and 6b show no all-region trend in onset of winter precipitation or October–November wet-day frequency during 1915–2018, the period covered by the daily precipitation record. The lack of trend in Figure 6a holds when other thresholds for winter onset are considered (25% or 50% of mean October–December precipitation total). CMIP5 models generally project fall drying (Pierce et al., 2013), with a delayed onset of the winter precipitation season and reduced October–November wet-day frequency (Figures 6a and 6b), but these simulated anthropogenic effects on the statewide mean were small as of 2018. The lack of all-region trends in observed fall precipitation timing and frequency is representative for North Coast, Sierra Nevada, and Central Coast (Figures S17–S19). In South Coast, the number of days to reach 10% of long-term mean October–December precipitation total increased by 2.5 days (6%) and the number of wet days per October–November decreased by 1.2 days (−18%) during 1915–2018 (Figure S20). These trends were insignificant but consistent in sign and magnitude with those of the CMIP5 multi-model mean, suggesting a possible continuation of these trends throughout the 21st century.

There is no evidence thus far of changes in the frequency or intensity of dry wind events in fall. There has been no observed statewide or regional trend in the number of fall days with high (top 15%) FFWI values

(Figure 6c) or in the mean FFWI among of the most intense 10 FWI days per fall (Figure S21a) since at least 1958, when our FFWI records begin (Figures S17–S20). Lack of observed trends in fall FFWI is also consistent with prior observations of Santa Ana wind events in southern California (Abatzoglou et al., 2013; Guzman-Morales et al., 2016). Extending the records from those studies through 2018, there were no significant trends in fall Santa Ana frequency or intensity since the mid-1900s (Figure S22), despite projected negative trends (Guzman-Morales & Gershunov, 2019; Hughes et al., 2011).

As evaporative demand is an important secondary driver of fuel moisture variability, warming should promote large fall wildfires, all else held equal. During 1896–2018, October–November Tmax increased significantly ($p < 0.05$) by 1.67 °C, driving an increase in VPD of 1.21 hPa (+14.6%; Figures 6d and 6e). This positive trend in VPD was not statistically significant, however, due to high interannual to decadal variability in fall temperature and humidity. VPD did increase significantly ($p < 0.05$) during 1948–2018, and this trend is almost entirely responsible for the decrease in FM1000 during this time. Since 1948, the frequency of low (bottom 15%) FM1000 days per fall increased significantly ($p < 0.01$) by 8.8 days (+67%; Figure 6f). Warming-driven increases in aridity also significantly reduced the lowest daily FM1000 values each fall (Figure S21b). Regionally, the increase in low FM1000 days was significant in all regions except South Coast, where high interannual and decadal variability in fall precipitation overwhelmed the warming signal (Figures S17–S20).

Despite a lack of trends in the primary controls on daily risk of large fall wildfires in California (precipitation and wind), VPD-driven decreases in FM1000 caused significant ($p < 0.05$) 1958–2018 increases in the all-region mean daily fall *Pfire* (Figure 6g), significantly increasing the number of high (top 15%) *Pfire* days per fall by 7.9 days (+59%; Figure 6h) as well as the mean of the highest 10 daily *Pfire* values each fall (Figure S21c). Recall that the *Pfire* record is constrained to 1958–2018 because of its reliance on FFWI. As was the case for FM1000, increases in fall *Pfire* were significant in all regions except South Coast. Importantly, the significant decline in FM1000 and increase in *Pfire* began in the mid-1900s, when VPD was particularly low relative to the early 1900s (Figure 6e). Given that fall VPD did not increase significantly over the past century in any region, it is likely that trends in fall FM1000 and *Pfire* have also been insignificant over the past century despite the significant trends since the mid-1900s.

In 2017 and 2018, all-region mean fall *Pfire* and number of fall days with high *Pfire* were higher than in any other year on record (Figures 6g and 6h), and the largest fires in these years occurred when *Pfire* was at or near record levels (Figure 4). Despite the strong role of decadal variability over the past century, fall VPD nonetheless increased in all four regions and continued anthropogenic warming will likely promote continued increases in the probability of large fall wildfires. However, this may be counteracted to some degree if offshore wind events reduce in intensity and frequency (Hughes et al., 2011).

3.4. Nonclimate Factors

The effects of climate on western United States wildfire have not occurred in isolation. Large wildfires require abundant fuels, aridity, ignitions, and wind (Bradstock, 2010). Although we find that the observed increases in summer forest-fire area since 1972 are very likely explained by warming-induced increases in VPD, the mean baseline sensitivity of wildfire activity during this study period may have been elevated due to an artificial twentieth-century buildup of fuels due to fire suppression (e.g., Harris & Taylor, 2015; Marlon et al., 2012; Minnich et al., 1995). Further, humans and human infrastructure greatly enhance the number of ignitions (Balch et al., 2017; Syphard et al., 2017). On the other hand, humans may have counteracted the fire-promoting effect of recent warming in some cases. For example, the frequency of human-started wildfires in California declined over the past two to four decades despite increased ignitions from power-related infrastructure, and urban expansion has reduced the area and connectivity of burnable wildlands (Balch et al., 2017; Keeley & Syphard, 2018; Sleeter et al., 2011). Additionally, the past century of frequent human-started fires in South Coast (where lightning is exceedingly rare), along with other human-caused disturbances such as urban expansion, has led to vegetation-type transitions in some areas (Keeley et al., 2005; Syphard et al., 2018) that may, depending on species, region, and microclimate, promote or limit continued increases in wildfire activity (Keeley et al., 2009; Parks et al., 2015). In the future, vegetation transitions may be increasingly impactful on wildfire trends (e.g., Hurteau et al., 2019; McKenzie & Littell, 2016).

4. Conclusions

California has been the geographic focus of extensive speculation among scientists, politicians, and media as to the biophysical and societal factors that have contributed to recent exceptional wildfires and large increases in wildfire activity in recent decades (e.g., Krieger, 2018; Pierre-Louis, 2018; Vore, 2018). Anthropogenic climate change is commonly debated as a driver of these recent wildfire changes, but there are many ways in which anthropogenic climate change could conceivably affect wildfire and many variables that wildfire in California is sensitive to. A nuanced understanding of how, when, where, and why California wildfire activity has increased in recent decades is critical for sustainable environmental and development decisions that specifically take into account how anthropogenic climate change is likely to proceed and affect wildfire across California's diverse landscapes. Our methods should be increasingly applicable to other regions globally, as governmental and satellite-based records of wildfire activity are steadily alleviating observational duration as a major limiting factor for empirical studies of wildfire.

In this study we evaluated the various possible links between anthropogenic climate change and observed changes in California wildfire activity across seasons, regions, and land cover types since the early 1970s. The clearest link between California wildfire and anthropogenic climate change thus far has been via warming-driven increases in atmospheric aridity, which works to dry fuels and promote summer forest fire, particularly in the North Coast and Sierra Nevada regions. Warming has been far less influential on summer wildfire in nonforest areas. In fall, the drivers of wildfire are particularly complex, but warming does appear to enhance the probability of large fall wildfires such as those in 2017 and 2018, and this effect is likely to grow in the coming decades.

Importantly, the effects of anthropogenic warming on California wildfire thus far have arisen from what may someday be viewed as a relatively small amount of warming. According to climate models, anthropogenic warming since the late 1800s has increased the atmospheric vapor-pressure deficit by approximately 10%, and this increase is projected to double by the 2060s. Given the exponential response of California burned area to aridity, the influence of anthropogenic warming on wildfire activity over the next few decades will likely be larger than the observed influence thus far where fuel abundance is not limiting.

Below, we conclude with executive summaries of our primary findings for summer wildfire in forests, summer wildfire in nonforests, and fall wildfire.

4.1. Summer, Forest

Annual statewide burned area increased significantly during 1972–2018, largely due to an eightfold increase in annual summer forest-fire extent, most of which occurred in the heavily forested North Coast and Sierra Nevada regions. Summer forest-fire extent is strongly dictated by heat and atmospheric aridity, which reduce snowpack and dry out fuels. Warm-season atmospheric aridity (vapor-pressure deficit) increased significantly across California since the late 1800s, driven largely by daytime warming of approximately 1.8 °C (1.4 °C since the early 1970s). Based on a regression analysis, the vast majority of the observed increase in summer forest-fire extent since 1972 is accounted for by observed significant increases in warm-season vapor-pressure deficit (caused by warming). Importantly, the sensitivity of burned area to aridity is modulated by background conditions such as fuel abundance and connectivity, ignition frequency, and resources dedicated toward suppression, all of which changed over the past century. However, the statistical relationship between vapor-pressure deficit and forest fire area remained stable during 1972–2018, supporting the interpretation that increased aridity was the primary driver of the increase in summer forest-fire area during this time. The observed rates of warming and increasing vapor-pressure deficit are consistent with those simulated by climate models when forced by anthropogenic emissions, indicating that these trends are extremely likely to continue for decades to come. *The large increase in California's annual forest-fire area over the past several decades is very likely linked to anthropogenic warming.*

4.2. Summer, Nonforest

Annual summer burned area did not increase in nonforest lands in the Central and South Coast regions, and increases in nonforest burned area were weak in the North Coast and Sierra Nevada. Summer nonforested burned area is most strongly promoted by high precipitation total in the year or two prior to the fire year,

reflecting the necessity of precipitation for growth of fine fuels that can facilitate fire spread in the subsequent year. Fire-year precipitation deficit and atmospheric aridity also appear to promote summer wildfire in these regions, but this effect is relatively weak. Over the past century, the frequency of wet years followed by dry years increased, which should have promoted nonforest summer wildfire. The lack of large increases in nonforest summer burned area may reflect the counteracting effects of the other factors such as human fire suppression, reduced ignitions, and reduced vegetation cover due to drought. Climate models do not represent the observed increase in interannual swings from wet to dry years as a robust result of anthropogenic climate change thus far. *The link between anthropogenic climate change and summer wildfire in nonforest appears weak thus far.*

4.3. Fall

Large fall wildfires became more frequent in California over the past several decades, mainly due to increases in the North Coast and Sierra Nevada regions. In all regions, large fall wildfires often occur when strong offshore wind events coincide with dry fuels. These conditions were extreme throughout California in 2017 and 2018, driving very large fall wildfires in all regions in one or both years. The character of offshore wind events did not change since records began in the mid-1900s. Climate models project these wind events to decrease in frequency and intensity in the future. Fall fuel moisture is dictated largely by fall precipitation, but nonetheless is calculated to have declined significantly since the mid-1900s due to warming. This warming-induced drying was likely caused by a combination of anthropogenic forcing and natural multidecade variability and caused an 8-day increase in the number of days per October–December with a high probability of large wildfires. This exemplifies an important secondary effect of background warming, which is projected to continue, on fall wildfires. In the South Coast, fall drying was also promoted by a small reduction in the frequency of fall precipitation, consistent with climate model projections. *The link between anthropogenic climate change and fall wildfire appears weaker than in summer thus far but is likely to strengthen if continued warming and possibly delayed onset of winter precipitation counteract projected decreases in the intensity and frequency of offshore wind events.*

Acknowledgments
All data sets used are publicly available, and the sources are listed in Table S1. A.P.W. was funded by Columbia University's Center for Climate and Life and the Zegar Family Foundation. We also acknowledge support from University of California Office of the President MRPI grant MRP-17-446315 (D.L., A.G., and J.G.M.), from NOAA via the CNAP RISA (D.L. and A.G.), from DOI via the Southwest Climate Adaptation Science Center grant G18AC00320 (A.G. and J.G.M.), the Visiting Scholar Program and Fire Centre Research Hub at the University of Tasmania (J.T.A.), Earth Lab through CIRES and the University of Colorado, Boulder's Grand Challenge Initiative (J.K.B.), and the USGS North Central Climate Adaptation Science Center (J.K.B.). LDEO publication 8332.

References

Abatzoglou, J. T. (2013). Development of gridded surface meteorological data for ecological applications and modelling. *International Journal of Climatology*, *33*(1), 121–131. https://doi.org/10.1002/joc.3413

Abatzoglou, J. T., Barbero, R., & Nauslar, N. J. (2013). Diagnosing Santa Ana winds in Southern California with synoptic-scale analysis. *Weather and Forecasting*, *28*(3), 704–710. https://doi.org/10.1175/WAF-D-13-00002.1

Abatzoglou, J. T., & Kolden, C. A. (2013). Relationships between climate and macroscale area burned in the western United States. *International Journal of Wildland Fire*, *22*(7), 1003–1020. https://doi.org/10.1071/WF13019

Abatzoglou, J. T., Kolden, C. A., Balch, J. K., & Bradley, B. A. (2016). Controls on interannual variability in lightning-caused fire activity in the western US. *Environmental Research Letters*, *11*(4). https://doi.org/10.1088/1748-9326/11/4/045005

Abatzoglou, J. T., Kolden, C. A., Williams, A. P., Lutz, J. A., & Smith, A. M. S. (2017). Climatic influences on interannual variability in regional burn severity across western US forests. *International Journal of Wildland Fire*, *26*(4), 269–275. https://doi.org/10.1071/WF16165

Abatzoglou, J. T., & Williams, A. P. (2016). Impact of anthropogenic climate change on wildfire across western US forests. *Proceedings of the National Academy of Sciences USA*, *113*(42), 11,770–11,775. https://doi.org/10.1073/pnas.1607171113

Abatzoglou, J. T., Williams, A. P., Boschetti, L., Zubkova, M., & Kolden, C. A. (2018). Global patterns of interannual climate-fire relationships. *Global Change Biology*, *24*(11), 5164–5175. https://doi.org/10.1111/gcb.14405

AghaKouchak, A., Ragno, E., Love, C., Moftakhari, H. (2018), Projected changes in California's precipitation intensity-duration-frequency curves. California's Fourth Climate Change Assessment, Rep. CCCA4-CEC-2018-005, 32 pp, California Energy Commission, Sacramento, CA. http://www.climateassessment.ca.gov/techreports/docs/20180827-Projections_CCCA4-CEC-2018-005.pdf.

Allen, R. G., Pereira, L. S., Raes, D., Smith, M. (1998), Crop evapotranspiration—Guidelines for computing crop water requirements-FAO Irrigation and drainage, paper 56. 15 pp, Food and Agriculture Organizatoin of the United Nations, Rome. http://www.fao.org/3/X0490E/X0490E00.htm.

Balch, J., Schoennagel, T., Williams, A. P., Abatzoglou, J., Cattau, M., Mietkiewicz, N., & St Denis, L. (2018). Switching on the big burn of 2017. *Fire*, *1*(1), 17. https://doi.org/10.3390/fire1010017

Balch, J. K., Bradley, B. A., Abatzoglou, J. T., Nagy, R. C., Fusco, E. J., & Mahood, A. L. (2017). Human-started wildfires expand the fire niche across the United States. *Proceedings of the National Academy of Sciences USA*, *114*(11), 2946–2951. https://doi.org/10.1073/pnas.1617394114

Barbero, R., Abatzoglou, J. T., Larkin, N. K., Kolden, C. A., & Stocks, B. (2015). Climate change presents increased potential for very large fires in the contiguous United States. *International Journal of Wildland Fire*, *24*(7), 892–899. https://doi.org/10.1071/WF15083

Barbero, R., Abatzoglou, J. T., Steel, E. A., & Larkin, N. K. (2014). Modeling very large-fire occurrences over the continental United States from weather and climate forcing. *Environmental Research Letters*, *9*(12). https://doi.org/10.1088/1748-9326/9/12/124009

Barnett, T., Pierce, D., Hidalgo, H., Bonfils, C., Santer, B., Das, T., et al. (2008). Human-induced changes in the hydrology of the western United States. *Science*, *319*(5866), 1080–1083. https://doi.org/10.1126/science.1152538

Batllori, E., Parisien, M. A., Krawchuk, M. A., & Moritz, M. A. (2013). Climate change-induced shifts in fire for Mediterranean ecosystems. *Global Ecology and Biogeography*, *22*(10), 1118–1129. https://doi.org/10.1111/geb.12065

Berg, N., & Hall, A. (2015). Increased interannual precipitation extremes over California under climate change. *Journal of Climate*, *28*(16), 6324–6334. https://doi.org/10.1175/JCLI-D-14-00624.1

Billmire, M., French, N. H. F., Loboda, T., Owen, R. C., & Tyner, M. (2014). Santa Ana winds and predictors of wildfire progression in southern California. *International Journal of Wildland Fire*, *23*(8), 1119–1129. https://doi.org/10.1071/WF13046

Bradstock, R. A. (2010). A biogeographic model of fire regimes in Australia: Current and future implications. *Global Ecology and Biogeography*, *19*(2), 145–158. https://doi.org/10.1111/j.1466-8238.2009.00512.x

CalFire (2018). http://www.fire.ca.gov/. Accessed June 23 2019.

Cohen, J. D., Deeming, J. E. (1985), The national fire-danger rating system: Basic equations, Rep. Gen. Tech. Rep. PSW-82, 16 pp, USFS, Pacific Southwest Forest and Range Experiment Station, Berkeley, CA. https://www.fs.fed.us/psw/publications/documents/psw_gtr082/psw_gtr082.pdf.

Conil, S., & Hall, A. (2006). Local regimes of atmospheric variability: A case study of Southern California. *Journal of Climate*, *19*(17), 4308–4325. https://doi.org/10.1175/JCLI3837.1

Daly, C., Gibson, W. P., Dogget, M., Smith, J., Taylor, G. (2004), Up-to-date monthly climate maps for the coterminous United States, paper presented at Proceedings of the 14th AMS Conference on Applied Climatology, 84th AMS Annual Meeting, American Meteorological Society, Seattle, WA, January 13-16, 2004.

Dennison, P. E., Brewer, S. C., Arnold, J. D., & Moritz, M. A. (2014). Large wildfire trends in the western United States, 1984–2011. *Geophysical Research Letters*, *41*, 2928–2933. https://doi.org/10.1002/2014GL059576

deVore, C. (2018). Trump's right about California's wildfires: It wasn't climate change; Two New California Laws Prove It, Forbes, November 27 2018. https://www.forbes.com/sites/chuckdevore/2018/11/27/trumps-right-about-californias-fires-it-wasnt-climate-change-two-new-california-laws-prove-it/

Dolanc, C. R., Thorne, J. H., & Safford, H. D. (2013). Widespread shifts in the demographic structure of subalpine forests in the Sierra Nevada, California, 1934 to 2007. *Global Ecology and Biogeography*, *22*(3), 264–276. https://doi.org/10.1111/j.1466-8238.2011.00748.x

Evan, A. T. (2019). A new method to characterize changes in the seasonal cycle of snowpack. *Journal of Applied Meteorology and Climatology*, *58*, 131–143. https://doi.org/10.1175/JAMC-D-18-0150.1

Fosberg, M. A. (1978), Weather in wildland fire management: The fire weather index, paper presented at Conference on Sierra Nevada Meteorology, American Meterological Society, South Lake Tahoe, CA, 19-21 June 1977.

Guzman-Morales, J., & Gershunov, A. (2019). Climate change suppresses Santa Ana winds of Southern California and sharpens their seasonality. *Geophysical Research Letters*, *46*(5), 2772–2780. https://doi.org/10.1029/2018GL080261

Guzman-Morales, J., Gershunov, A., Theiss, J., Li, H., & Cayan, D. (2016). Santa Ana Winds of Southern California: Their climatology, extremes, and behavior spanning six and a half decades. *Geophysical Research Letters*, *43*, 2827–2834. https://doi.org/10.1002/2016GL067887

Harris, L., & Taylor, A. H. (2015). Topography, fuels, and fire exclusion drive fire severity of the Rim Fire in an old Growth mixed-conifer forest, Yosemite National Park, USA. *Ecosystems*, *18*(7), 1192–1208. https://doi.org/10.1007/s10021-015-9890-9

Higuera, P. E., Abatzoglou, J. T., Littell, J. S., & Morgan, P. (2015). The changing strength and nature of fire-climate relationships in the Northern Rocky Mountains, USA, 1902-2008. *PloS ONE*, *10*(6). https://doi.org/10.1371/journal.pone.0127563

Holden, Z. A., Swanson, A., Luce, C. H., Jolly, W. M., Maneta, M., Oyler, J. W., et al. (2018). Decreasing fire season precipitation increased recent western US forest wildfire activity. *Proceedings of the National Academy of Sciences USA*, *115*(36), E8349–E8357. https://doi.org/10.1073/pnas.1802316115

Hughes, M., & Hall, A. (2010). Local and synoptic mechanisms causing Southern California's Santa Ana winds. *Climate Dynamics*, *34*(6), 847–857. https://doi.org/10.1007/s00382-009-0650-4

Hughes, M., Hall, A., & Kim, J. (2011). Human-induced changes in wind, temperature and relative humidity during Santa Ana events. *Climatic Change*, *109*(1), 119–132. https://doi.org/10.1007/s10584-011-0300-9

Hurteau, M. D., Liang, S., Westerling, A. L., & Wiedinmyer, C. (2019). Vegetation-fire feedback reduces projected area burned under climate change. *Scientific reports*, *9*(1), 2838. https://doi.org/10.1038/s41598-019-39284-1

Jin, Y., Goulden, M. L., Faivre, N., Veraverbeke, S., Sun, F., Hall, A., et al. (2015). Identification of two distinct fire regimes in Southern California: Implications for economic impact and future change. *Environmental Research Letters*, *10*(9). https://doi.org/10.1088/1748-9326/10/9/094005

Jin, Y., Randerson, J. T., Faivre, N., Capps, S., Hall, A., & Goulden, M. L. (2014). Contrasting controls on wildland fires in Southern California during periods with and without Santa Ana winds. *Journal of Geophysical Research: Biogeosciences*, *119*, 432–450. https://doi.org/10.1002/2013JG002541

Kalnay, E., Kanamitsu, M., Kistler, R., Collins, W., Deaven, D., Gandin, L., et al. (1996). The NCEP/NCAR 40-year reanalysis project. *Bulletin of the American Meteorological Society*, *77*(3), 437–471.

Keeley, J. E. (2004). Impact of antecedent climate on fire regimes in coastal California. *International Journal of Wildland Fire*, *13*(2), 173–182. https://doi.org/10.1071/WF03037

Keeley, J. E., Baer-Keeley, M., & Fotheringham, C. J. (2005). Alien plant dynamics following fire in Mediterranean-climate California shrublands. *Ecological Applications*, *15*(6), 2109–2125. https://doi.org/10.1890/04-1222

Keeley, J. E., & Fotheringham, C. J. (2001). Historic fire regime in southern California shrublands. *Conservation Biology*, *15*(6), 1536–1548. https://doi.org/10.1046/j.1523-1739.2001.00097.x

Keeley, J. E., Safford, H., Fotheringham, C. J., Franklin, J., & Moritz, M. (2009). The 2007 southern California wildfires: Lessons in complexity. *Journal of Forestry*, *107*(6), 287–296. https://doi.org/10.1093/jof/107.6.287

Keeley, J. E., & Syphard, A. D. (2016). Climate change and future fire regimes: Examples from California. *Geosciences*, *6*(3), 37. https://doi.org/10.3390/geosciences6030037

Keeley, J. E., & Syphard, A. D. (2017). Different historical fire–climate patterns in California. *International Journal of Wildland Fire*, *26*(4), 253–268. https://doi.org/10.1071/WF16102

Keeley, J. E., & Syphard, A. D. (2018). Historical patterns of wildfire ignition sources in California ecosystems. *International Journal of Wildland Fire*, *27*(12), 781–799. https://doi.org/10.1071/WF18026

Kitzberger, T., Falk, D. A., Westerling, A. L., & Swetnam, T. W. (2017). Direct and indirect climate controls predict heterogeneous early-mid 21st century wildfire burned area across western and boreal North America. *PloS one*, *12*(12). https://doi.org/10.1371/journal.pone.0188486

Klimaszewski-Patterson, A., Weisberg, P. J., Mensing, S. A., & Scheller, R. M. (2018). Using paleolandscape modeling to investigate the impact of Native American–Set fires on pre-Columbian forests in the Southern Sierra Nevada, California, USA. *Annals of the American Association of Geographers*, *108*(6), 1635–1654. https://doi.org/10.1080/24694452.2018.1470922

Krawchuk, M., Moritz, M. (2012), Fire and climate change in California: Changes in the distribution and frequency of fire in climates of the future and recent past (1911-2099). 58 pp, California Energy Commission, Berkeley, CA. https://www.energy.ca.gov/2012publications/CEC-500-2012-026/CEC-500-2012-026.pdf.

Krieger, L. M. (2018), California's wildfires: What's the cause? Us, The Mercury News, August 12 2018. https://www.mercurynews.com/2018/08/12/whats-starting-all-these-fires-we-are/.

Lehner, F., Deser, C., Simpson, I. R., & Terray, L. (2018). Attributing the US Southwest's recent shift into drier conditions. *Geophysical Research Letters*, *45*, 6251–6261. https://doi.org/10.1029/2018GL078312

Liang, S., Hurteau, M. D., & Westerling, A. L. (2017). Response of Sierra Nevada forests to projected climate-wildfire interactions. *Global Change Biology*, *23*(5), 2016–2030. https://doi.org/10.1111/gcb.13544

Littell, J. S. (2018). Drought and fire in the Western USA: Is climate attribution enough? *Current Climate Change Reports*, *4*(4), 396–406. https://doi.org/10.1007/s40641-018-0109-y

Littell, J. S., McKenzie, D., Peterson, D. L., & Westerling, A. L. (2009). Climate and wildfire area burned in Western US ecoprovinces, 1916-2003. *Ecological Applications*, *19*(4), 1003–1021. https://doi.org/10.1890/07-1183.1

Littell, J. S., McKenzie, D., Wan, H. Y., & Cushman, S. A. (2018). Climate change and future wildfire in the western United States: An ecological approach to nonstationarity. *Earth's Future*, *6*(8), 1097–1111. https://doi.org/10.1029/2018EF000878

Livneh, B., Bohn, T. J., Pierce, D. W., Munoz-Arriola, F., Nijssen, B., Vose, R., et al. (2015). A spatially comprehensive, hydrometeorological data set for Mexico, the US, and Southern Canada 1950–2013. *Scientific Data*, *2*(1). https://doi.org/10.1038/sdata.2015.42

Livneh, B., Rosenberg, E. A., Lin, C., Nijssen, B., Mishra, V., Andreadis, K. M., et al. (2013). A long-term hydrologically based dataset of land surface fluxes and states for the conterminous United States: Update and extensions. *Journal of Climate*, *26*(23), 9384–9392. https://doi.org/10.1175/JCLI-D-12-00508.1

Maloney, E. D., Camargo, S. J., Chang, E., Colle, B., Fu, R., Geil, K. L., et al. (2013). North American climate in CMIP5 experiments: Part III: Assessment of twenty-first century projections. *Journal of Climate*, *27*(6), 2230–2270. https://doi.org/10.1175/JCLI-D-13-00273.1

Mann, M. L., Batllori, E., Moritz, M. A., Waller, E. K., Berck, P., Flint, A. L., et al. (2016). Incorporating anthropogenic influences into fire probability models: Effects of human activity and climate change on fire activity in California. *PLoS One*, *11*(4). https://doi.org/10.1371/journal.pone.0153589

Marlier, M. E., Xiao, M., Engel, R., Livneh, B., Abatzoglou, J. T., & Lettenmaier, D. P. (2017). The 2015 drought in Washington State: A harbinger of things to come? *Environmental Research Letters*, *12*(11), 114008. https://doi.org/10.1088/1748-9326/aa8fde

Marlon, J. R., Bartlein, P. J., Gavin, D. G., Long, C. J., Anderson, R. S., Briles, C. E., et al. (2012). Long-term perspective on wildfires in the western USA. *Proceedings of the National Academy of Sciences USA*, *109*(9), E535–E543. https://doi.org/10.1073/pnas.1112839109

Matthews, S. (2014). Dead fuel moisture research: 1991–2012. *International Journal of Wildland Fire*, *23*(1), 78–92. https://doi.org/10.1071/WF13005

McKenzie, D., & Littell, J. S. (2016). Climate change and the eco-hydrology of fire: Will area burned increase in a warming western USA? *Ecological Applications*, *27*(1), 26–36. https://doi.org/10.1002/eap.1420

Menne, M. J., Durre, I., Vose, R. S., Gleason, B. E., & Houston, T. G. (2012). An overview of the global historical climatology network-daily database. *Journal of Atmospheric and Oceanic Technology*, *29*(7), 897–910. https://doi.org/10.1175/JTECH-D-11-00103.1

Minnich, R. A., Barbour, M. G., Burk, J. H., & Fernau, R. F. (1995). Sixty years of change in Californian conifer forests of the San Bernardino Mountains. *Conservation Biology*, *9*(4), 902–914. https://doi.org/10.1046/j.1523-1739.1995.09040902.x

Monteith, J. L. (1965). Evaporation and environment. *Symoposia of the Society for Experimental Biology*, *19*, 205–234. http://www.unc.edu/courses/2007fall/geog/801/001/www/ET/Monteith65.pdf

Moritz, M. A., Moody, T. J., Krawchuk, M. A., Hughes, M., & Hall, A. (2010). Spatial variation in extreme winds predicts large wildfire locations in chaparral ecosystems. *Geophysical Research Letters*, *37*, L04081. https://doi.org/10.1029/2009GL041735

Mote, P. W., Li, S., Lettenmaier, D. P., Xiao, M., & Engel, R. (2018). Dramatic declines in snowpack in the western US. *npj Climate and Atmospheric Science*, *1*(1). https://doi.org/10.1038/s41612-018-0012-1

Nagy, R., Fusco, E., Bradley, B., Abatzoglou, J. T., & Balch, J. (2018). Human-related ignitions increase the number of large wildfires across US ecoregions. *Fire*, *1*(1), 4. https://doi.org/10.3390/fire1010004

Nauslar, N. J., Abatzoglou, J. T., & Marsh, P. T. (2018). The 2017 North Bay and Southern California Fires: A case study. *Fire*, *1*(1), 18. https://doi.org/10.3390/fire1010018

Parks, S. A., Miller, C., Parisien, M.-A., Holsinger, L. M., Dobrowski, S. Z., & Abatzoglou, J. (2015). Wildland fire deficit and surplus in the western United States, 1984-2012. *Ecosphere*, *6*(12), 1–13. https://doi.org/10.1890/ES15-00294.1

Pendergrass, A. G., Knutti, R., Lehner, F., Deser, C., & Sanderson, B. M. (2017). Precipitation variability increases in a warmer climate. *Scientific Reports*, *7*(1), 17,966. https://doi.org/10.1038/s41598-017-17966-y

Pierce, D. W., Das, T., Cayan, D. R., Maurer, E. P., Miller, N. L., Bao, Y., et al. (2013). Probabilistic estimates of future changes in California temperature and precipitation using statistical and dynamical downscaling. *Climate Dynamics*, *40*(3-4), 839–856. https://doi.org/10.1007/s00382-012-1337-9

Pierce, D. W., Kalansky, J. F., Cayan, D. R. (2018), Climate, drought, and sea level rise scenarios. California's Fourth Climate Change Assessment, Rep. CNRA-CEC-2018-006, 78 pp, California Energy Commission, Sacramento, CA. http://www.climateassessment.ca.gov/techreports/docs/20180827-Projections_CCCA4-CEC-2018-006.pdf.

Pierre-Louis, K. (2018), Why does California have so many wildfires?, The New York Times, November 9, 2018. https://www.nytimes.com/2018/11/09/climate/why-california-fires.html.

Polade, S. D., Gershunov, A., Cayan, D. R., Dettinger, M. D., & Pierce, D. W. (2017). Precipitation in a warming world: Assessing projected hydro-climate changes in California and other Mediterranean climate regions. *Scientific Reports*, *7*(1), 10,783. https://doi.org/10.1038/s41598-017-11285-y

Polade, S. D., Pierce, D. W., Cayan, D. R., Gershunov, A., & Dettinger, M. D. (2014). The key role of dry days in changing regional climate and precipitation regimes. *Scientific Reports*, *4*, 4364. https://doi.org/10.1038/srep04364

Radeloff, V. C., Helmers, D. P., Kramer, H. A., Mockrin, M. H., Alexandre, P. M., Bar-Massada, A., et al. (2018). Rapid growth of the US wildland-urban interface raises wildfire risk. *Proceedings of the National Academy of Sciences USA*, *115*(13), 3314–3319. https://doi.org/10.1073/pnas.1718850115

Raphael, M. N. (2003). The Santa Ana winds of California. *Earth Interactions*, *7*(8), 1–13. https://doi.org/10.1175/1087-3562(2003)007<0001:TSAWOC>2.0.CO;2

Romps, D. M., Seeley, J. T., Vollaro, D., & Molinari, J. (2014). Projected increase in lightning strikes in the United States due to global warming. *Science*, *346*(6211), 851–854. https://doi.org/10.1126/science.1259100

Seager, R., Cane, M., Henderson, N., Lee, D.-E., Abernathy, R., & Zhang, H. (2019). Strengthening tropical Pacific zonal sea surface temperature gradient consistent with greenhouse gases. *Nature Climate Change*, *9*, 517–522. https://doi.org/10.1038/s41558-019-0505-x

Sen, P. B. (1968). Estimates of the regression coefficient based on Kendall's Tau. *Journal of the American Statistical Association*, *63*(324), 1379–1389. https://doi.org/10.1080/01621459.1968.10480934

Simpson, I. R., Seager, R., Ting, M., & Shaw, T. A. (2016). Causes of change in Northern Hemisphere winter meridional winds and regional hydroclimate. *Nature Climate Change*, *6*, 65–70. https://doi.org/10.1038/nclimate2783

Sleeter, B. M., Wilson, T. S., Soulard, C. E., & Liu, J. (2011). Estimation of late twentieth century land-cover change in California. *Environmental Monitoring and Assessment*, *173*(1-4), 251–266. https://doi.org/10.1007/s10661-010-1385-8

Stephens, S. L., & Ruth, L. W. (2005). Federal forest-fire policy in the United States. *Ecological Applications*, *15*(2), 532–542. https://doi.org/10.1890/04-0545

Sun, F., Walton, D., & Hall, A. (2015). A hybrid dynamical-statistical downscaling technique, part II: End-of-century warming projections predict a new climate state in the Los Angeles region. *Journal of Climate*, *28*, 4618–4636. https://doi.org/10.1175/JCLI-D-14-00197.1

Swain, D. L., Langenbrunner, B., Neelin, J. D., & Hall, A. (2018). Increasing precipitation volatility in twenty-first-century California. *Nature Climate Change*, *8*, 427–433. https://doi.org/10.1038/s41558-018-0140-y

Swetnam, T. W. (1993). Fire history and climate change in giant sequoia groves. *Science*, *262*(5135), 885–889. https://doi.org/10.1126/science.262.5135.885

Swetnam, T. W., & Baisan, C. H. (1996). Historical fire regime patterns in the southwestern United States since AD 1700. In C. D. Allen (Ed.), *Fire Effects in Southwestern Fortest: Proceedings of the 2nd La Mesa Fire Symposium* (pp. 11–32). Rocky Mountain Research Station: USDA Forest Service. http://digitalcommons.usu.edu/barkbeetles/85/

Swetnam, T. W., & Baisan, C. H. (2003). Tree-ring reconstructions of fire and climate history in the Sierra Nevada and Southwestern United States. In T. T. Veblen, W. L. Baker, G. Montenegro, & T. W. Swetnam (Eds.), *Fire and climatic change in temperate ecosystems of the western Americas* (pp. 158–195). New York: Springer. https://link.springer.com/content/pdf/10.1007/b97443.pdf

Swetnam, T. W., & Betancourt, J. L. (1998). Mesoscale disturbance and ecological response to decadal climatic variability in the American Southwest. *Journal of Climate*, *11*(12), 3128–3147. https://doi.org/10.1175/1520-0442(1998)011<3128:MDAERT>2.0.CO;2

Syphard, A. D., Gershunov, A., Lawson, D. M., Rivera-Huerta, H., Guzman-Moralez, J., Jennings, M. K. (2018). San Diego wildfires: Drivers of change and future outlook. San Diego County Ecosystems: Ecological Impacts Of Climate Change On A Biodiversity Hotspot. California's Fourth Climate Change Assessment, 15-17 pp, California Energy Commission, Sacramento, CA. http://sdrufc.com/wp-content/uploads/2018/06/ClimateSciAlliance_EcosystemAssessment_36p_mar18.pdf.

Syphard, A. D., Keeley, J. E., Pfaff, A. H., & Ferschweiler, K. (2017). Human presence diminishes the importance of climate in driving fire activity across the United States. *Proceedings of the National Academy of Sciences USA*, *114*(52), 13,750–13,755. https://doi.org/10.1073/pnas.1713885114

Syphard, A. D., Rustigian-Romsos, H., Mann, M., Conlisk, E., Moritz, M. A., & Ackerly, D. (2019). The relative influence of climate and housing development on current and projected future fire patterns and structure loss across three California landscapes. *Global Environmental Change*, *56*, 41–55. https://doi.org/10.1016/j.gloenvcha.2019.03.007

Taylor, A. H., Trouet, V., Skinner, C. N., & Stephens, S. (2016). Socioecological transitions trigger fire regime shifts and modulate fire–climate interactions in the Sierra Nevada, USA, 1600–2015 CE. *Proceedings of the National Academy of Sciences USA*, *113*(48), 13,684–13,689. https://doi.org/10.1073/pnas.1609775113

Taylor, K. E., Stouffer, R. J., & Meehl, G. A. (2012). An overview of CMIP5 and the experiment design. *Bulletin of the American Meteorological Society*, *93*(4), 485–498. https://doi.org/10.1175/BAMS-D-11-00094.1

van Vuuren, D. P., Edmonds, J., Kainuma, M., Riahi, K., Thomson, A., Hibbard, K., et al. (2011). The representative concentration pathways: An overview. *Climatic Change*, *109*(1-2), 5–31. https://doi.org/10.1007/s10584-011-0148-z

Vose, R. S., Applequist, S., Squires, M., Durre, I., Menne, M. J., Williams, C. N. Jr., et al. (2014). Improved historical temperature and precipitation time series for US climate divisions. *Journal of Applied Meteorology and Climatology*, *53*(5), 1232–1251. https://doi.org/10.1175/JAMC-D-13-0248.1

Walton, D. B., Sun, F., Hall, A., & Capps, S. (2015). A hybrid dynamical-statistical downscaling technique, part I: Development and validation of a technique. *Journal of Climate*, *28*, 3597–4617. https://doi.org/10.1175/JCLI-D-14-00196.1

Westerling, A. L. (2016). Increasing western US forest wildfire activity: Sensitivity to changes in the timing of spring. *Philosophical Transactions of the Royal Society B*, *371*(1696). https://doi.org/10.1098/rstb.2015.0178

Westerling, A. L. (2018), Wildfire simulations for California's fourth climate change assessment: Projecting Changes in Extreme Wildfire Events with a Warming Climate. California's Fourth Climate Change Assessment, Rep. CCCA4-CEC-2018-014, 57 pp, California Energy Commission. http://www.climateassessment.ca.gov/techreports/docs/20180827-Projections_CCCA4-CEC-2018-014.pdf

Westerling, A. L., & Bryant, B. P. (2008). Climate change and wildfire in California. *Climatic Change*, *87*(1), 231–249. https://doi.org/10.1007/s10584-007-9363-z

Westerling, A. L., Bryant, B. P., Preisler, H. K., Holmes, T. P., Hidalgo, H. G., Das, T., & Shrestha, S. R. (2011). Climate change and growth scenarios for California wildfire. *Climatic Change*, *109*(1), 445–463. https://doi.org/10.1007/s10584-011-0329-9

Westerling, A. L., Cayan, D. R., Brown, T. J., Hall, B. L., & Riddle, L. G. (2004). Climate, Santa Ana winds and autumn wildfires in southern California, *Eos. Transactions American Geophysical Union*, *85*(31), 289–296. https://doi.org/10.1029/2004EO310001

Westerling, A. L., Gershunov, A., Brown, T. J., Cayan, D. R., & Dettinger, M. D. (2003). Climate and wildfire in the western United States. *Bulletin of the American Meteorological Society*, *84*(5), 595–604. https://doi.org/10.1175/BAMS-84-5-595

Westerling, A. L., Hidalgo, H. G., Cayan, D. R., & Swetnam, T. W. (2006). Warming and earlier spring increase western US forest wildfire activity. *Science*, *313*(5789), 940–943. https://doi.org/10.1126/science.1128834

Williams, A. P., & Abatzoglou, J. T. (2016). Recent advances and remaining uncertainties in resolving past and future climate effects on global fire activity. *Current Climate Change Reports*, *2*(1), 1–14. https://doi.org/10.1007/s40641-016-0031-0

Williams, A. P., Cook, B. I., Smerdon, J. E., Bishop, D. A., Seager, R., & Mankin, J. S. (2017). The 2016 southeastern US drought: An extreme departure from centennial wetting and cooling. *Journal of Geophysical Research: Atmospheres*, *122*, 10,888–10,905. https://doi.org/10.1002/2017JD027523

Williams, A. P., Gentine, P., Moritz, M. A., Roberts, D. A., & Abatzoglou, J. T. (2018). Effect of reduced summer cloud shading on evaporative demand and wildfire in coastal southern California. *Geophysical Research Letters*, *45*, 5653–5662. https://doi.org/10.1029/2018GL077319

Williams, A. P., Schwartz, R. E., Iacobellis, S., Seager, R., Cook, B. I., Still, C. J., et al. (2015). Urbanization causes increased cloud-base height and decreased fog in coastal southern California. *Geophysical Research Letters*, *42*, 1527–1536. https://doi.org/10.1002/2015GL063266

Williams, A. P., Seager, R., Abatzoglou, J. T., Cook, B. I., Smerdon, J. E., & Cook, E. R. (2015). Contribution of anthropogenic warming to California drought during 2012–2014. *Geophysical Research Letters*, *42*, 6819–6828. https://doi.org/10.1002/2015GL064924

Williams, A. P., Seager, R., Macalady, A. K., Berkelhammer, M., Crimmins, M. A., Swetnam, T. W., et al. (2015). Correlations between components of the water balance and burned area reveal new insights for predicting fire activity in the southwest US. *International Journal of Wildland Fire*, *24*(1), 14–26. https://doi.org/10.1071/WF14023

Earth's Future

Supporting Information for

Observed impacts of anthropogenic climate change on wildfire in California

A. Park Williams[1], John T. Abatzoglou[2], Alexander Gershunov[3], Janin Guzman-Morales[3], Daniel A. Bishop[1,4], Jennifer K. Balch[5], Dennis P. Lettenmaier[6]

[1]Lamont-Doherty Earth Observatory of Columbia University; Palisades, NY 10964, USA
[2]Department of Geography; University of Idaho, Moscow; Moscow, ID 83844
[3]Scripps Institution of Oceanography; University of California, San Diego; La Jolla, CA 92093
[4]Department of Earth and Environmental Sciences; Columbia University, New York, NY 10027
[5]Earth Lab/CIRES & Department of Geography; University of Colorado Boulder; Boulder, CO 80309
[6]Department of Geography; University of California, Los Angeles; Los Angeles, CA 90095

Corresponding author: A. Park Williams (williams@ldeo.columbia.edu)

Contents of this file

Text S1: Definition of California regions

For each of the four regions considered (North Coast, Sierra Nevada, Central Coast, South Coast), we merged Bailey ecoregions at the section level. For *North Coast*, we merged the Klamath Mountains and Northern California Coast sections. For *Sierra Nevada*, we merged the Sierra Nevada Foothills, Sierra Nevada, and Southern Cascades sections. For *Central Coast*, we merged the Central California Coast sections. For *South Coast*, we merged the Southern California Mountains and Valleys section with the Southern California coast sections.

Text S2: California wildfire data

The primary dataset was from CalFire Fire Resource and Assessment Program (version 17_1). For large fires during 1984–2016, we replaced CalFire burned areas with those from the more spatially resolved, Monitoring Trends in Burn Severity dataset (MTBS), a satellite-based record of wildfires at least 404 ha in size. We also included MTBS fires not represented by the CalFire database. The CalFire and MTBS datasets provide boundaries of the burned areas, which we clipped at the boundaries of the regions of interest. We then added wildfires from the multi-agency datasets (Table S1), excluding fires already considered from the CalFire and MTBS datasets. CalFire and multi-agency wildfire records end in 2017 (as of 11 March 2019). For 2018, we extracted wildfire polygons from Geomac. For intra-seasonal analyses of individual wildfires, we constrain our analyses to 1972–2017 because the Geomac dataset does not contain many smaller wildfires. For evaluation of forest-fire area, we used a gridded map at 1/120° resolution of forest fraction, developed from the Environmental Site Potential (ESP) product of LANDFIRE. ESP is a 30-m gridded classification of likely vegetation type given the biophysical environment. As in *Abatzoglou and Williams* (2016), we considered forest area to be represented by ESP grid cells classified as "forest" or "woodland." For each wildfire we estimated the forest area burned as the area of the wildfire multiplied by the area-weighted forest fraction among all grid cells that fall within the wildfire boundary. For interagency wildfires without polygon boundaries, we assumed the fires were circles centered on the reported location.

Text S3: Monthly gridded climate data

Monthly grids of mean daily maximum temperature (Tmax), daily minimum temperature (Tmin), and precipitation total for 1895–2018 came from the National Oceanic and Atmospheric Administration Climgrid dataset (*Vose et al.*, 2014). Monthly gridded mean dew point came from PRISM (*Daly et al.*, 2004), as Climgrid does not provide humidity data. PRISM is not used for precipitation and temperature because Climgrid has more stringent record-length requirements than PRISM, making Climgrid more appropriate for evaluation of trends. Monthly mean vapor pressure deficit (VPD) was calculated as saturation vapor pressure (calculated from Tmax and Tmin) minus actual vapor pressure (calculated from dew point for the observational record and from specific humidity and surface pressure for CMIP5 records). Seasonal precipitation anomalies were expressed as the standardized precipitation index (SPI). For a supplemental analysis, monthly mean wind, solar, and reference evapotranspiration (ETo) data come from *Williams et al.* (2017). ETo was calculated using the Penman-Monteith approach (*Monteith*, 1965) following the approach of the Food and Agriculture Organization of the United Nations (*Allen et al.*, 1998).

Text S4: Daily gridded fuel moisture and fire weather indices

Daily gridded surface meteorological data from gridMET (*Abatzoglou*, 2013) were used to calculate 1000-hour dead fuel moisture (FM1000) and the Fosberg Fire Weather index (FFWI). The 1000-hour dead fuel moisture (FM1000) was calculated using the US National Fire Danger Rating System (*Cohen and Deeming*, 1985). Calculations of FM1000 and FFWI require daily maximum and minimum humidity and temperature, wind speed, precipitation, and downward shortwave flux at the surface. The primary source of the daily data, gridMET, covers the period 1979-present. We extended these records back to 1948 using daily data from the NCEP-NCAR reanalysis (*Kalnay et al.*, 1996) and monthly data from Climgrid. Daily data from NCEP-NCAR reanalysis for the period 1948-2010 at a 2.5-degree resolution grid were bilinearly interpolated to the gridMET grid. Departures from monthly averages for temperature and dewpoint temperature, and the fraction of monthly precipitation per day were calculated. The daily departures were then added (temperature and dewpoint temperature) or multiplied (precipitation) to ClimGrid monthly data. Finally, we used a quantile mapping approach to bias correct these data to gridMET data of these same variables using monthly temporal bins. The quantile mapping approach ensures that the distribution of daily data for the 1979-2010 period of these data match those of the same period for gridMET, with pre-1979 data adhering to the same quantile correction procedures. For wind speed and downward shortwave radiation, we applied quantile mapping directly to interpolated fields from NCEP-NCAR data without any intermediary correction. Finally, we calculated daily minimum and maximum relative humidity using bias corrected fields of mean daily maximum and minimum temperature and dewpoint and applied a final quantile mapping procedure to ensure that the resultant relative humidity fields followed the same distribution for gridMET.

Text S5: Daily precipitation data

Daily weather station precipitation totals were extracted from the US subset of the daily Global Historical Climatology Network (GHCN) version 3.25 (*Menne et al.*, 2012; accessed 21 Feb 2019). Daily records were mainly used for analysis of daily precipitation frequency and timing of onset of the winter rainy season. We initially considered all California records that had at least 6 months of ≥90% daily coverage for at least 30 years during 1972–2018 (the period of overlap with the wildfire record) or at least one fall month with at least 95% of daily precipitation totals in at least 50% of years during both 1915–1966 and 1967–2018 (for evaluation of long-term trends in the timing of onset of the winter precipitation season). Fifty-two stations met either or both of these criteria in California. Missing daily values for these stations were estimated using calibrated (quantile matching) precipitation totals from the nearby station (100 km) found to most accurately estimate the target station's precipitation totals. The optimal station selected for gap filling and quantile-matching calibration parameters was determined on a rolling 25-day basis (e.g., gap filling for 13 Aug 2000 would be done using 1–25 Aug of all available years). Gap filling was only performed if correlation was reasonably strong ($r \geq 0.7$) between estimated and measured daily precipitation totals during the period of overlap. A small number of remaining data gaps were filled with calibrated values from the daily PRISM dataset for 1980–2018 and from the updated and merged *Livneh et al.* (2013; 2015) 1/16° gridded daily product for 1915–1979.

For analyses, we excluded stations that required heavy gap filling. For correlation between seasonal wet-day frequency (days with ≥2.54 mm precipitation) and warm-season burned area, we considered the gap-filled records from the 47 stations for which the original (pre-filled)

records had at least 90% of daily values per month in at least 5 of the warm-season (Mar-Oct) months for at least 70% of years during 1972–2018. For evaluation of trends in fall wet-day frequency and timing of onset of winter precipitation, we considered the gap-filled records from the 35 stations for which the original records had at least 90% of daily values for each of the fall months (Oct-Dec) in at least 70% of years during 1915–2018. Results reported in the paper were not sensitive to the criteria used for station selection. We did not consider daily precipitation records prior to 1915 due to a scarcity of stations with pre-1915 records and this is when the *Livneh et al.* datasets used for gap filling begin.

All seasonal or annual time series based on daily station data were made at the station level and these records were then aggregated to the regional scale. Each station was assigned to the region it was closest to. Stations east of the Sierra Nevada or South Coast regions were not considered, as these stations are located in deserts and their records generally agreed poorly with the rest of the records.

Table S1. Data sources

California Regions and landcover	
Bailey Ecoregions	https://www.sciencebase.gov/catalog/item/54244abde4b037b608f9e23d
LANDFIRE Environmental Site Potential	https://www.landfire.gov/esp.php
Wildfire	
CalFire wildfire boundaries 1901–2017	http://frap.fire.ca.gov/data/frapgisdata-sw-fireperimeters_download
MTBS wildfire grids 1984–2016	https://www.mtbs.gov
Multi-agency wildfire occurrences 1972–2017	http://fam.nwcg.gov/fam-web/weatherfirecd/state_data
Geomac 2018 wildfire boundaries	https://www.geomac.gov
Climate	
NOAA Climgrid 1895–2018 monthly; 1/24° resolution	ftp://ftp.ncdc.noaa.gov/pub/data/climgrid
PRISM 1895–2018 monthly; 1/24° resolution	http://prism.oregonstate.edu
Williams et al. (2017) grids of wind speed, solar radiation, and reference evapotranspiration 1895–2018 monthly; 1/8° resolution	https://www.ldeo.columbia.edu/~williams/seus_drought_jgr/forcing/
Global Historical Climatology Network 1915–2019 daily; station precipitation	https://www.ncdc.noaa.gov/ghcn-daily-description
Livneh Gridded Climate Data 1915–2015 daily; 1/16° resolution	ftp://livnehpublicstorage.colorado.edu/public/Livneh.2016.Dataset
GridMET 1979–2018 daily; 1/24° resolution	http://www.climatologylab.org/gridmet.html
CMIP5 Modeled Climate Data 1850–2100 monthly; spatial resolution is model-specific	https://esgfnode.llnl.gov/projects/cmip5

Table S2. CMIP5 models, and the number of runs per model, considered for each variable and emissions scenario.

Model	Monthly						Daily	
	Precipitation		Tmax & Tmin		VPD		Precipitation	
	Hist	RCP8.5	Hist	RCP8.5	Hist	RCP8.5	Hist	RCP8.5
ACCESS1-0	1	1	3	1	1	1	1	1
ACCESS1-3	1	1	3	1	1	1	1	1
BCC-CSM1-1	3	1	3	1	3	1	1	1
BCC-CSM1-1-M	3	1	3	1	3	1	1	1
BNU-ESM	1	1	-	-	-	-	1	1
CANESM2	5	5	5	5	5	5	1	1
CCSM4	6	6	8	6	6	6	1	1
CESM1-BGC	1	1	1	1	1	1	-	-
CESM1-CAM5	3	3	3	3	3	3	1	1
CESM1-CAM5-1-FV2	4	1	-	-	-	-	-	-
CESM1-WACCM	4	3	7	3	4	3	-	-
CMCC-CESM	1	1	1	1	-	-	-	-
CMCC-CM	1	1	-	-	-	-	1	1
CMCC-CMS	1	1	1	1	-	-	1	1
CNRM-CM5	10	5	10	5	10	5	1	1
CSIRO-MK3-6-0	10	10	10	10	10	10	1	1
EC-EARTH	1	1	9	10	-	-	-	-
FGOALS-G2	5	1	5	1	5	1	1	1
FGOALS-S2	3	3	-	-	-	-	-	-
FIO-ESM	3	3	-	-	-	-	-	-
GFDL-CM3	5	1	5	1	5	1	1	1
GFDL-ESM2G	3	1	1	1	1	1	1	1
GFDL-ESM2M	1	1	1	1	1	1	1	1
GISS-E2-H	11	4	18	5	10	3	-	-
GISS-E2-H-CC	1	1	1	1	1	1	-	-
GISS-E2-R	16	4	24	5	16	4	-	-
GISS-E2-R-CC	1	1	1	1	1	1	-	-
HADGEM2-AO	1	1	1	1	1	1	1	1
HADGEM2-CC	3	3	3	3	3	3	1	1
HADGEM2-ES	4	4	5	4	4	4	1	1
INMCM4	1	1	1	1	1	1	1	1
IPSL-CM5A-LR	6	4	6	4	5	4	1	1
IPSL-CM5A-MR	3	1	3	1	3	1	1	1
IPSL-CM5B-LR	1	1	1	1	1	1	1	1
MIROC-ESM	3	1	3	1	3	1	1	1
MIROC-ESM-CHEM	1	1	1	1	1	1	1	1
MIROC5	5	3	5	3	5	3	1	1
MPI-ESM-LR	3	3	3	3	-	-	1	1
MPI-ESM-MR	3	1	3	1	-	-	1	1
MRI-CGCM3	5	1	5	1	4	1	1	1
MRI-ESM1	1	1	-	-	-	-	-	-
NORESM1-M	3	1	3	1	3	1	1	1
NORESM1-ME	1	1	-	-	-	-	-	-

***Table S3**. Coefficients and goodness of fit statistics for regional logistic regression models in which 1000-hour dead fuel moisture (FM1000) and Fosberg Fire Weather Index (FFWI) are used to estimate daily probability of at least one large fall wildfire. Large wildfires are defined as the largest 15% of all fall wildfires in each region during 1972–2017.*

	Coefficient	***SE***	***T-statistic***	***p-Value***
North Coast				
Intercept	-1.2930199	0.57366258	-2.2539728	0.024197876
FM1000	-0.20723179	0.024964739	-8.3009796	1.0325641e-16
FFWI	0.071888089	0.018780241	3.8278577	0.00012926344
Chi^2 statistic vs constant model: 148, p-value = $7.52x10^{-33}$				
Sierra Nevada				
Intercept	-1.3845077	0.46187544	-2.9975779	0.0027213427
FM1000	-0.23822500	0.022372041	-10.648335	1.7751119e-26
FFWI	0.10219500	0.019689776	5.1902571	2.1000409e-07
Chi^2 statistic vs constant model: 205, p-value = $2.8x10^{-45}$				
Central Coast				
Intercept	-3.1800294	1.1312249	-2.8111382	0.0049366583
FM1000	-0.29936144	0.064260505	-4.6585603	3.1842856e-06
FFWI	0.16371052	0.036136780	4.5303020	5.8899423e-06
Chi^2 statistic vs constant model: 57.7, p-value = $2.98x10^{-13}$				
South Coast				
Intercept	-1.7282447	0.60040563	-2.8784618	0.0039961962
FM1000	-0.36874011	0.047818977	-7.7111669	1.2467222e-14
FFWI	0.15400192	0.016739862	9.1997128	3.5890727e-20
Chi^2 statistic vs constant model: 163, p-value = $5.02x10^{-36}$				

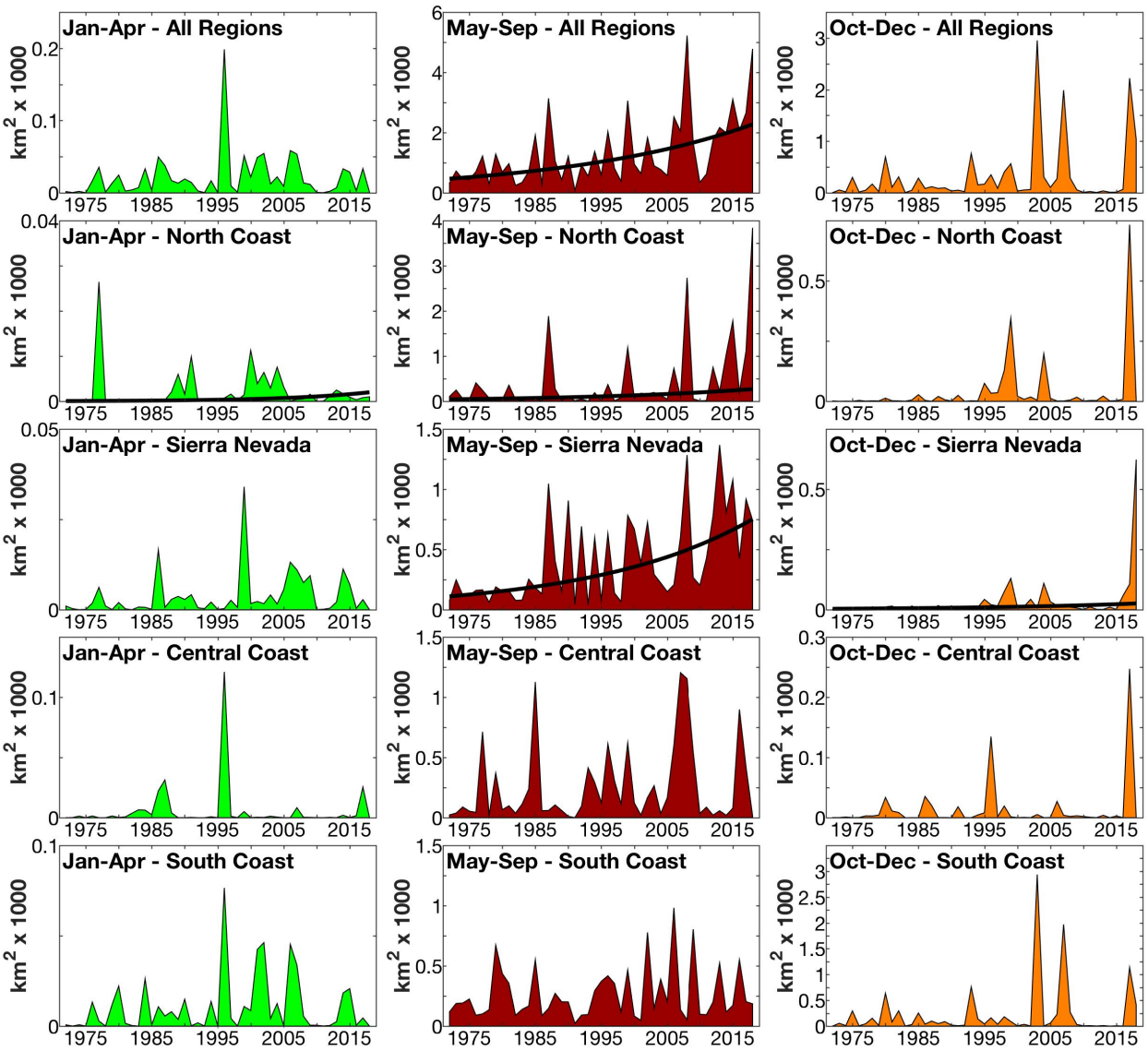

Figure S1. Seasonal burned areas in California regions for 1972–2018. Thiel-Sen trend lines are shown if found significant ($p<0.05$) by each of two non-parametric tests: Spearman Rank and Kendall's tau. Due to the exponential distribution of burned areas, trends were assessed for time series of the logarithm of annual burned area.

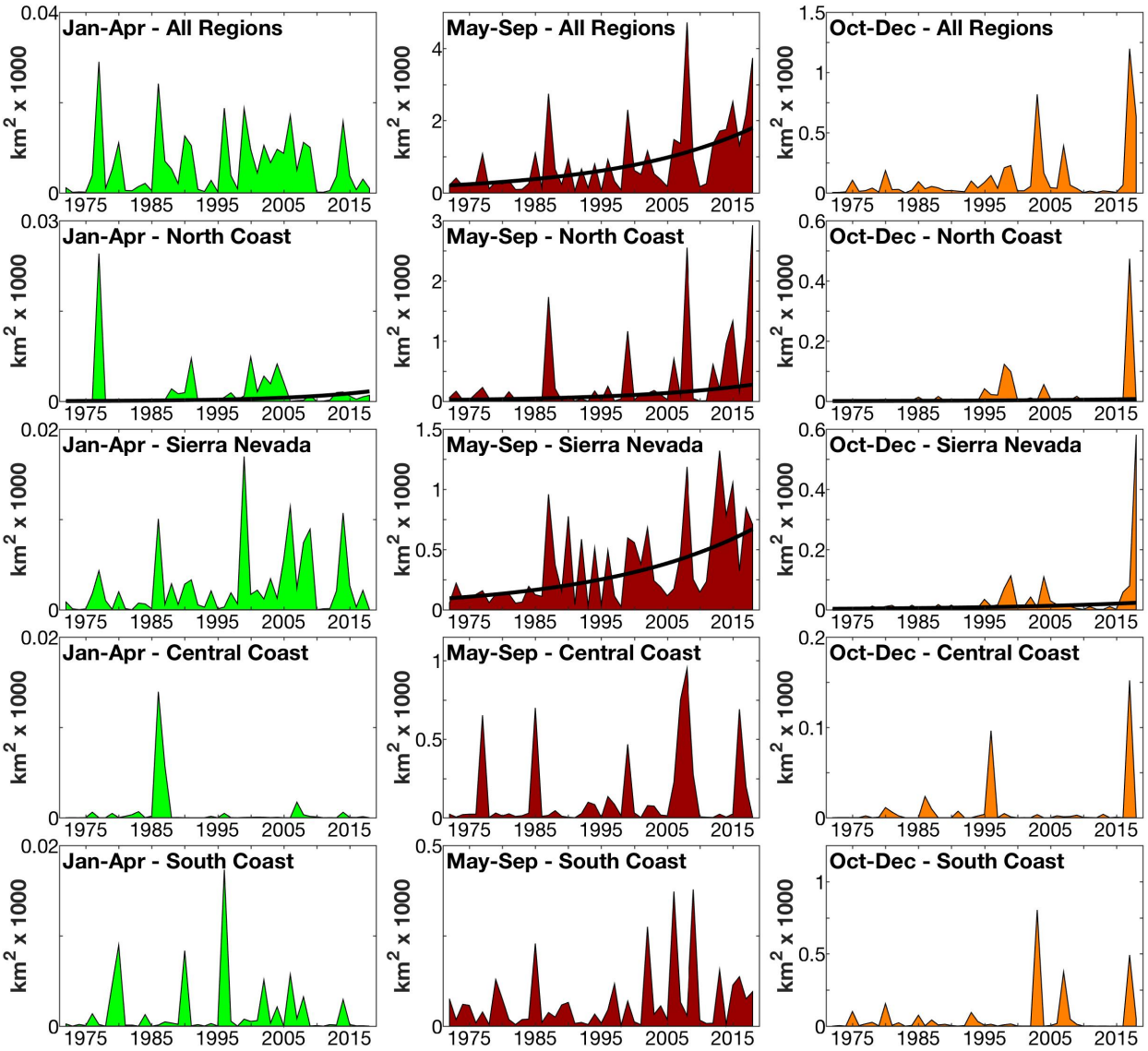

Figure S2. Seasonal forest-fire area in California regions for 1970–2018. Thiel-Sen trend lines are shown if found significant ($p<0.05$) by each of two non-parametric tests: Spearman Rank and Kendall's tau. Due to the exponential distribution of burned areas, trends were assessed for time series of the logarithm of annual burned area.

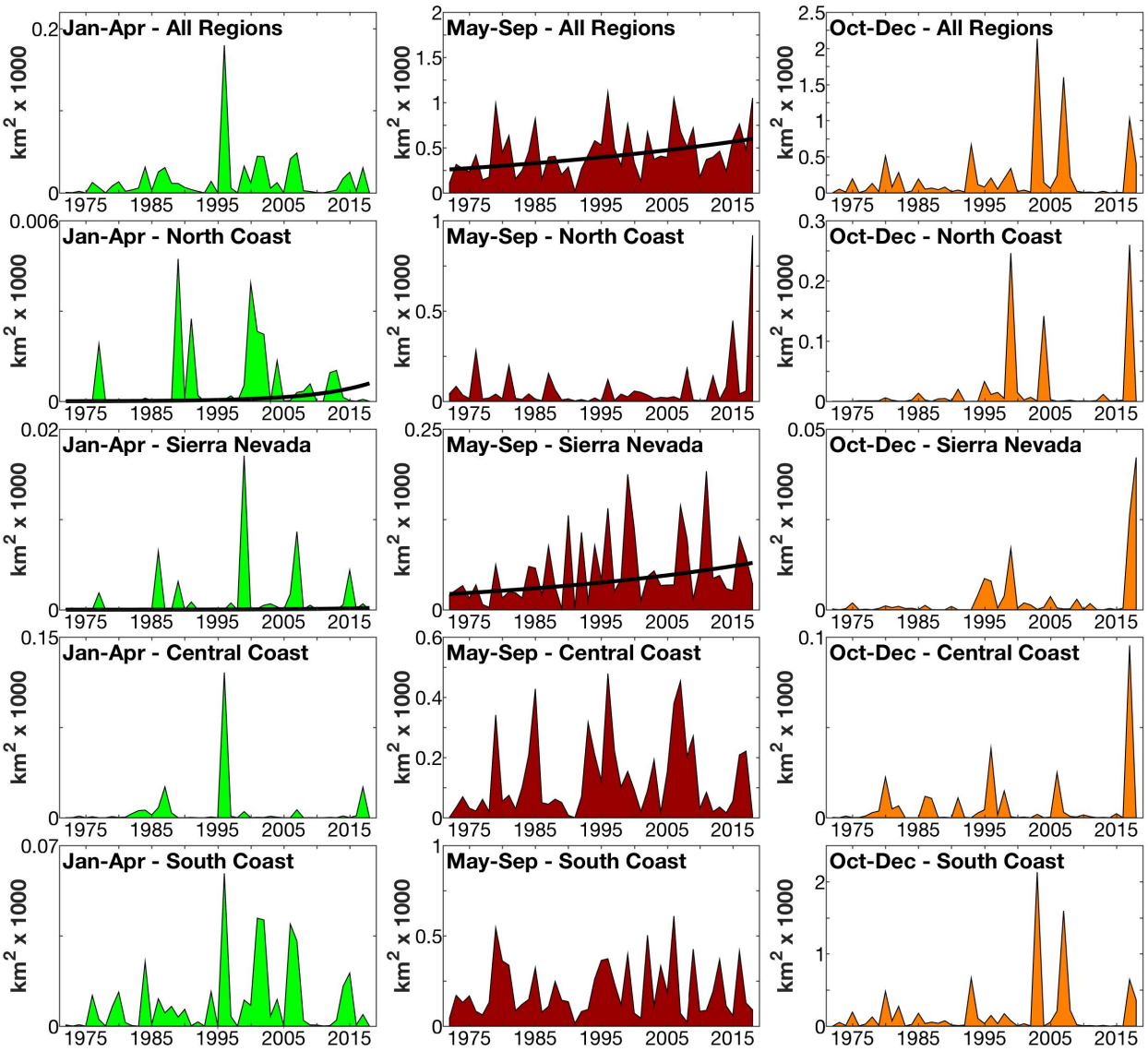

Figure S3. Seasonal non-forest burned areas in California regions for 1970–2018. Thiel-Sen trend lines are shown if found significant ($p<0.05$) by each of two non-parametric tests: Spearman Rank and Kendall's tau. Due to the exponential distribution of burned areas, trends were assessed for time series of the logarithm of annual burned area.

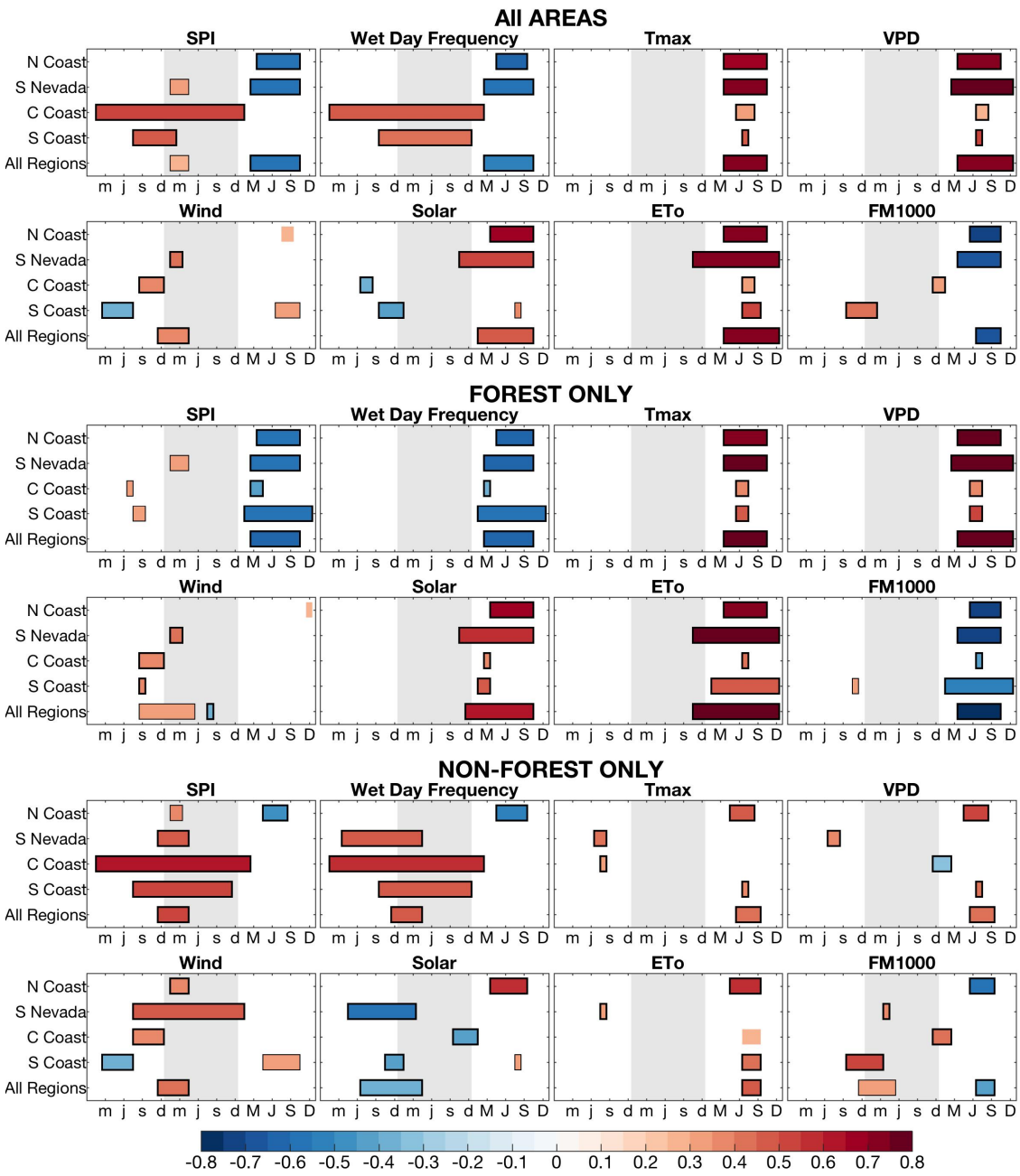

Figure S4. Optimal correlations between regional climate and summer log(burned area): 1972–2018. X-axis: month during which prior- and current-year mean climate conditions correlate with summer burned area, with prior-year climate beginning in winter two years before the wildfire year and extending through the wildfire year. Lowercase and uppercase: prior- and current-year months, respectively; M: March, J: June, S: September, D: December). Grey background shading is for visual assistance, indicating the one year prior to the wildfire year. Horizontal bars: consecutive months of optimal correlation. Thick and thin boundaries: significant correlation ($p<0.01$ and $p<0.05$, respectively). Significant secondary relationships of opposing sign are also shown. SPI: standardized precipitation index; Wet Day Frequency: frequency of days with precipitation ≥2.54 mm; Tmax: daily maximum temperature; VPD: vapor pressure deficit; Wind: wind speed; Solar: downward solar radiation at the surface; ETo: Penman-Monteith short-grass reference evapotranspiration; FM1000: 1000-hour dead fuel moisture.

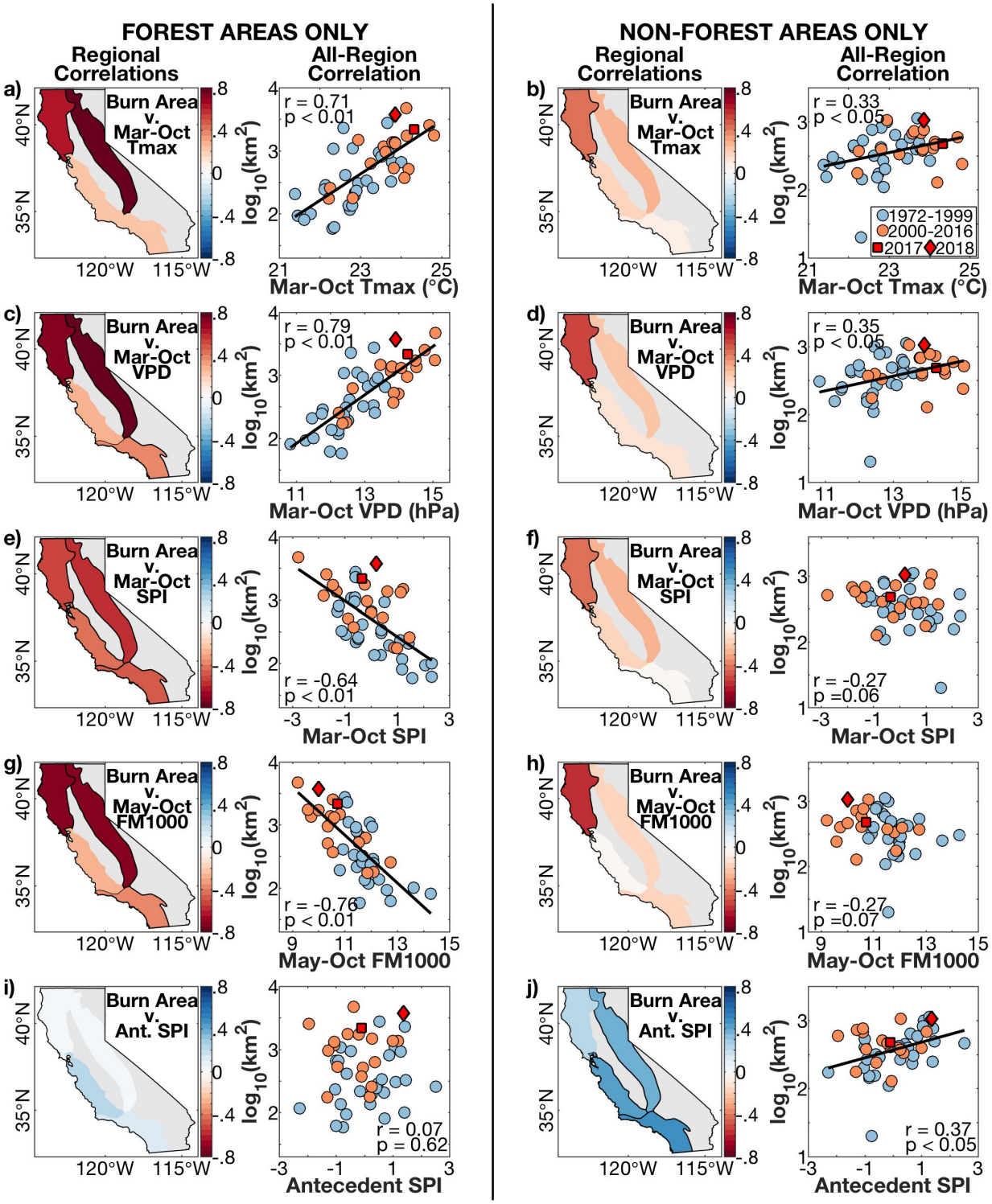

Figure S5. Correlation between climate and summer log(burned area) in (left) forested areas and (right) non-forested areas. Maps: regional correlations. Scatterplots: full study domain. Climate variables are (a,b) Mar-Oct mean daily maximum temperature (Tmax), (c,d) Mar-Oct vapor pressure deficit (VPD), (e,f) Mar-Oct standardized precipitation index (SPI), (g,h) May-Oct 1000-hour dead fuel moisture (FM1000), and (i,j) antecedent SPI from March of two years prior to October of the year prior. Regions are outlined in maps if correlation is significant at $p<0.05$.

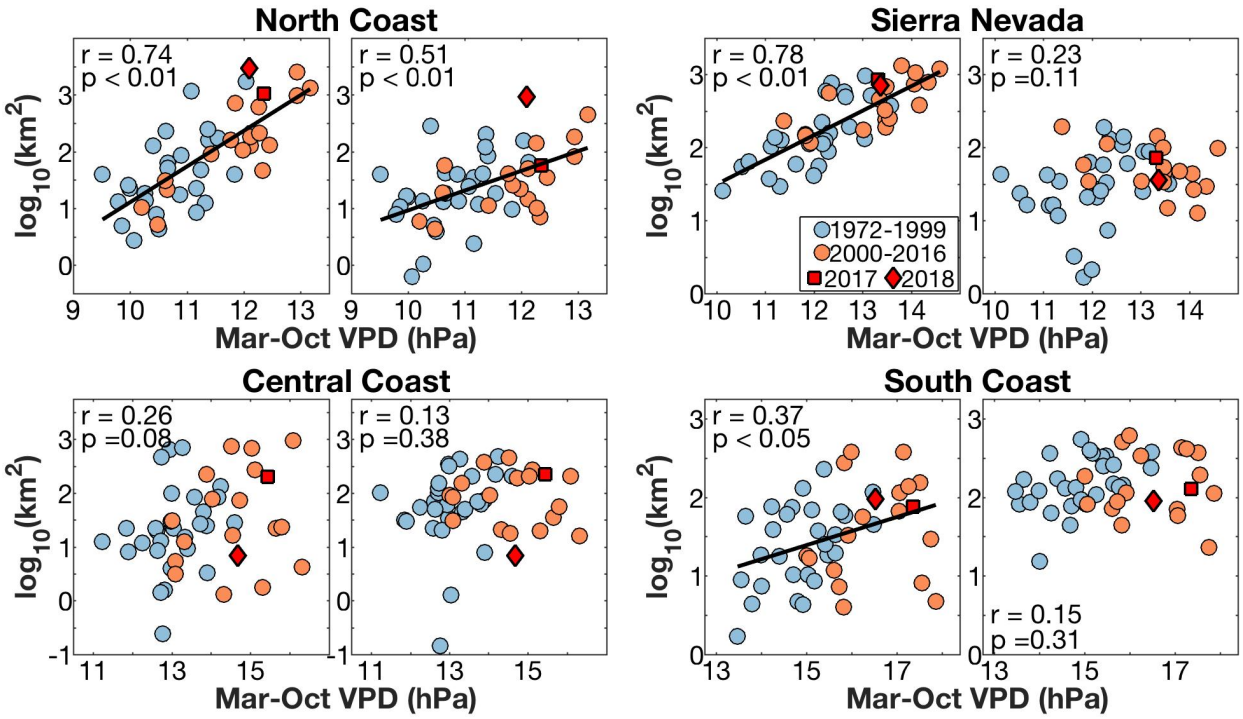

Figure S6. For each region, correlation between Mar-Oct vapor-pressure deficit (VPD) and summer log(burned area) in (left) forest and (right) non-forest.

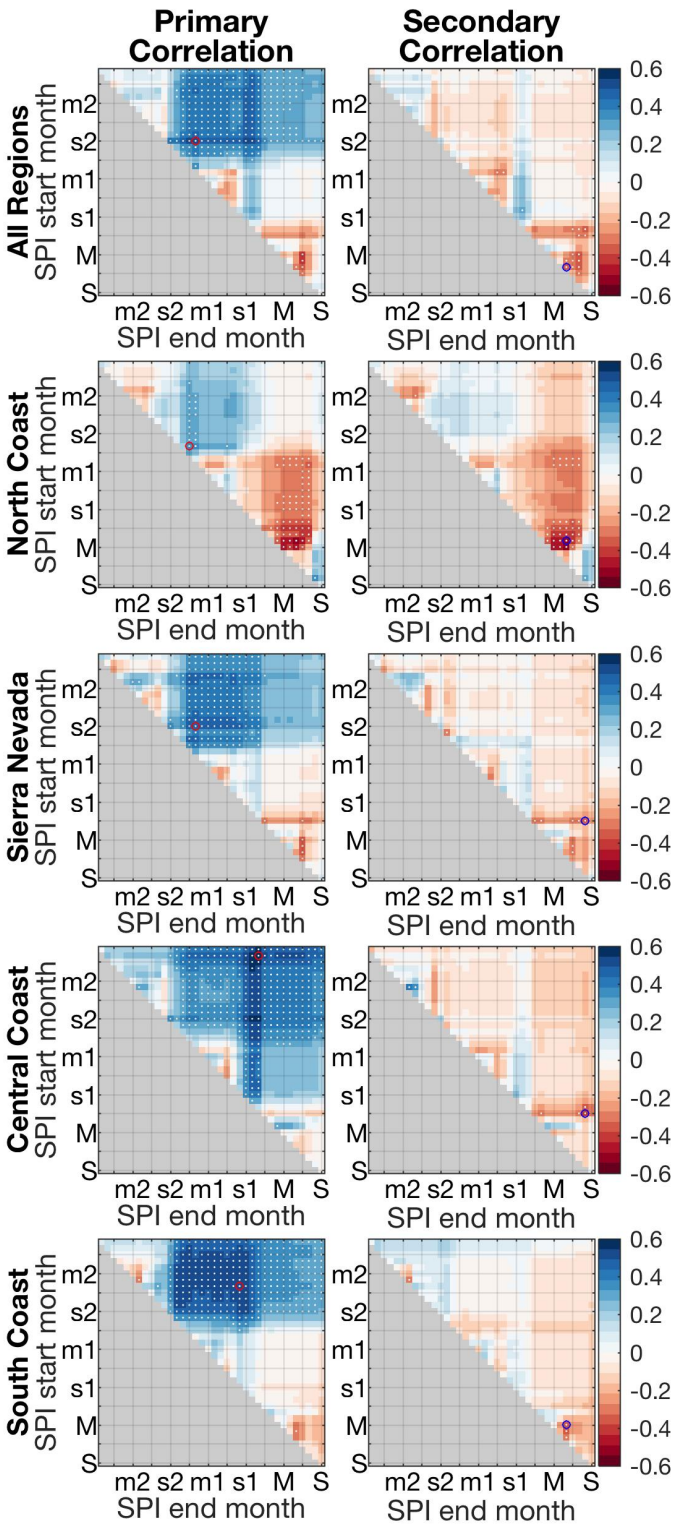

Figure S7. Correlation between summer non-forest log(burned area) and standardized precipitation index (SPI) during 1972–2018. (left) Original correlation. (right) Residual correlation after the maximum correlation in the left plot has been statistically removed from the burned-area record. A correlation is calculated between the burned-area records and an SPI record for each range of consecutive months in the 36-month period beginning in January of two

years prior to the fire year. On the x- and y-axes, lower-case values (m and s) represent March and September of 2 and 1 year prior to the fire year. Upper-case values represent the same months of the current year. White dots indicate Pearson correlation significance values p<0.05. In left plots, the red circle indicates the peak correlation between burned area and antecedent SPI. In right plots, the blue circle indicates the most negative correlation between burned area and current-year SPI.

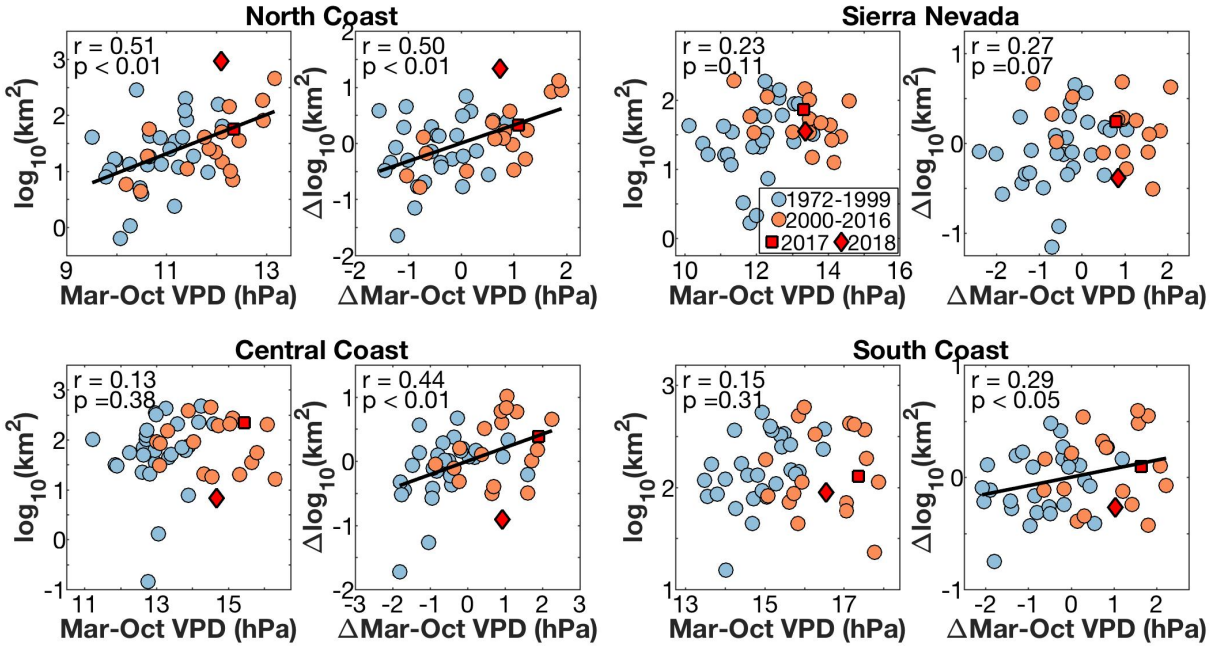

Figure S8. Correlation between annual summer non-forest log(burned area) and Mar-Oct vapor-pressure deficit (VPD) in each region. The right-hand scatter plot in each pair shows the relationship after removing correlation with antecedent standardized precipitation index (SPI) during the range of months when SPI correlates most positively with summer non-forest burned area (Fig. S7).

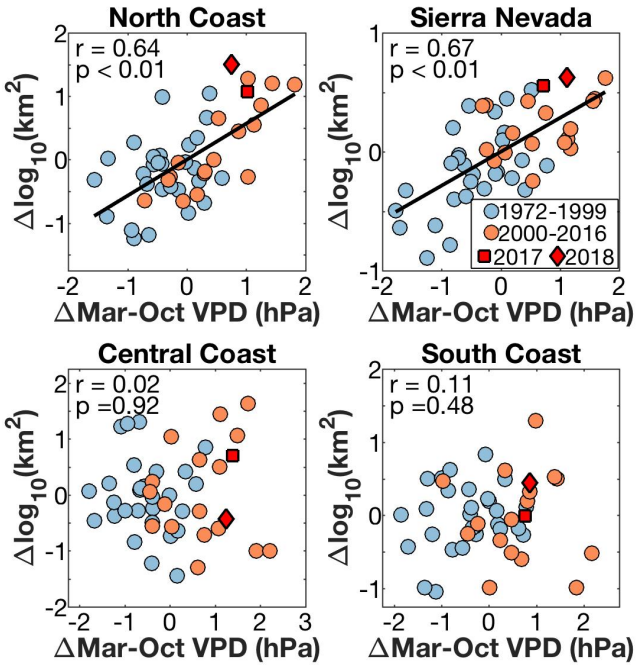

Figure S9. Correlation between annual summer forest log(burned area) and Mar-Oct vapor-pressure deficit (VPD) in each region after removing correlation with Mar-Oct standardized precipitation index from both variables.

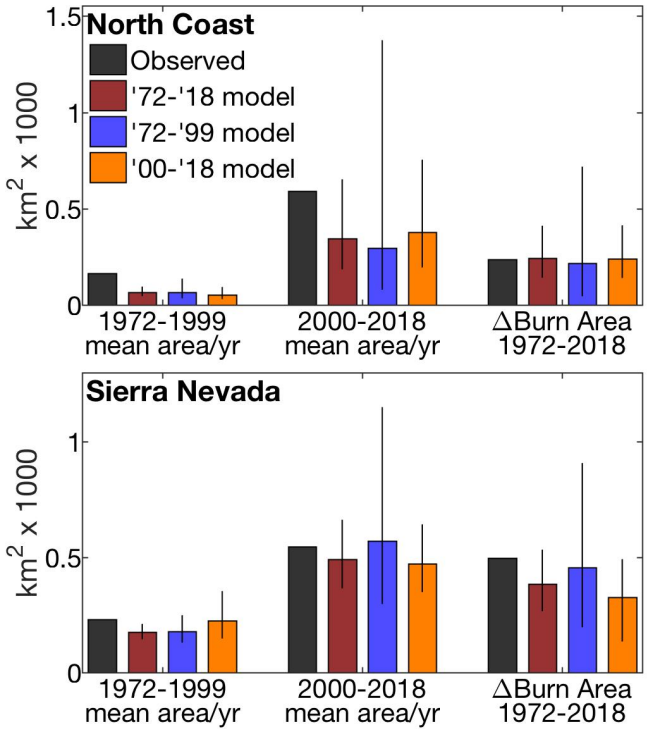

Figure S10. Stability of the influence of warm-season (Mar-Oct) vapor-pressure deficit (VPD) on summer (May-Sep) forest fire area. For each heavily forested region (North Coast and Sierra Nevada), a regression model was calculated to estimate summer forest-fire area based on warm-season VPD using data from each of three periods: 1972–2018 ('72-'18 model), 1972–1999 ('72-'99 model), and 2000–2018 ('00-'18 model). These models were used to estimate mean summer forest-fire per year during (left) 1972–1999 and (middle) 2000–2018. They were also used to estimate the effect of increasing VPD on the trend in summer forest-fire area (right). Whiskers bound 95% confidence intervals. In all cases, estimates based on the three VPD-based models are not significantly different.

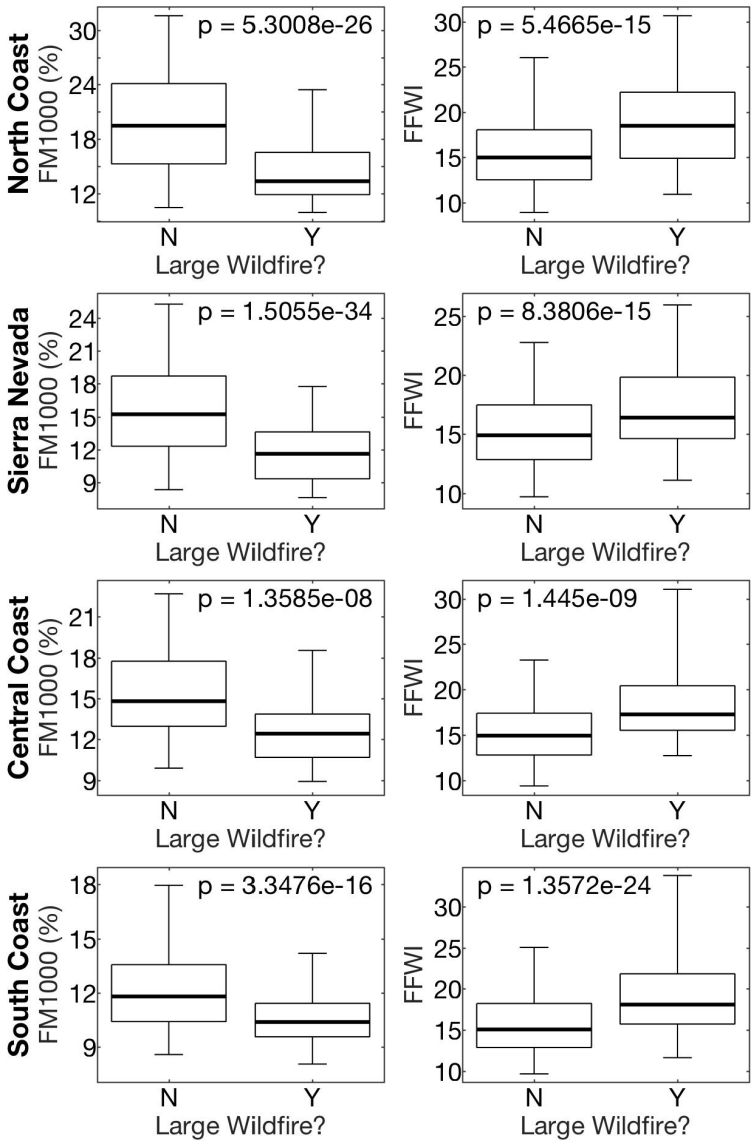

Figure S11. Box plots of daily (left) 1000-hour dead fuel moisture (FM1000) and (right) Fosberg Fire Weather Index (FFWI) on days without (N) and with (Y) large fall (Oct–Dec) wildfires in each region. Large fall wildfires are defined as the largest 15% of fires ≥0.1 ha during 1972–2017 in a given region. In boxplots, bold lines are median values, boxes bound interquartiles, and whiskers bound the inner 95% of values. P-values indicate probability that the two sets of daily values were drawn from the same distribution of daily values according to a one-way analysis of variance.

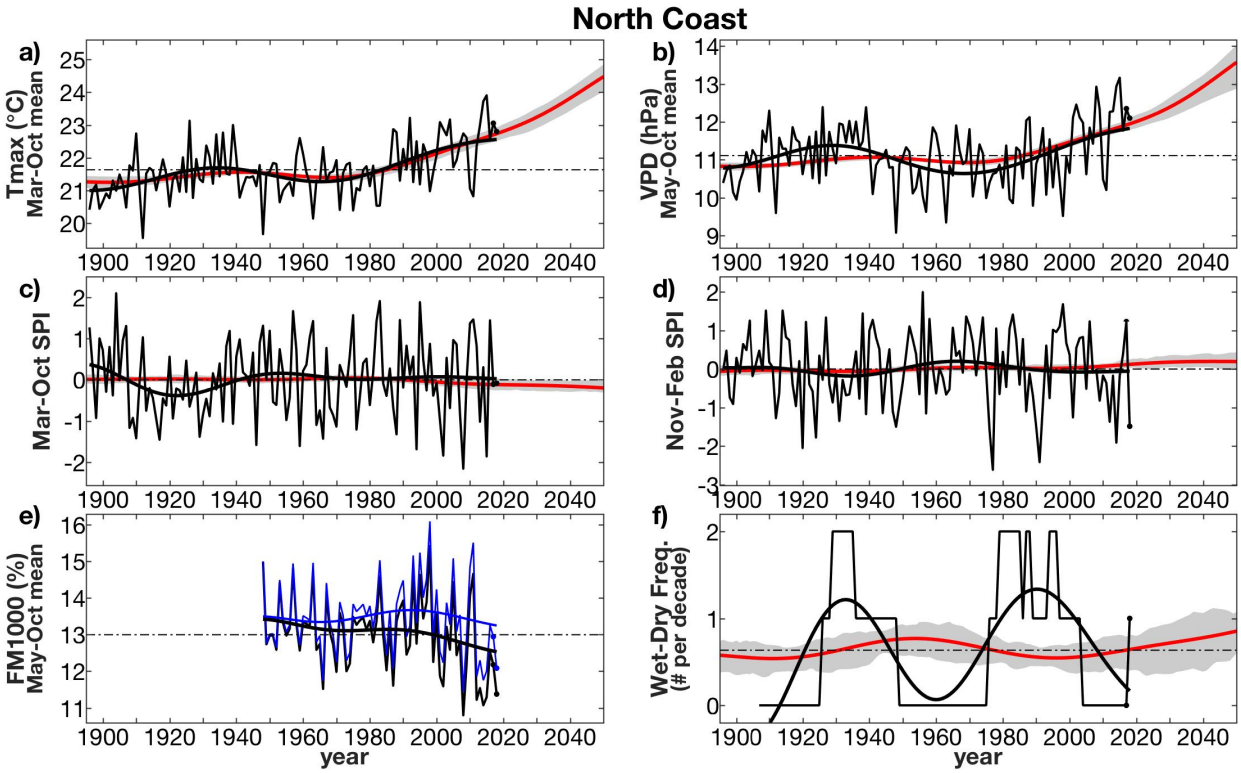

Figure S12. Summer climate trends in the North Coast region: Trends in climate variables important to California summer wildfire. (a-c) Mar-Oct mean daily maximum temperature (Tmax), vapor pressure deficit (VPD), and standardized precipitation index (SPI), respectively. (d) Nov-Feb SPI. (e) May–Oct mean 1000-hour dead fuel moisture (FM1000). (f) Number of "wet-dry" events per decade, when at least one of the 2 years preceding a dry water year was a wet water year. Water year: Oct–Sep. Wet and dry water years, respectively: water-year precipitation total greater and lower than the 80th and 20th percentiles of a 1921–2000 baseline. Black time series: observations (2017–2018 indicated with black dots) and (bold curve) 50-year low-pass filter. Blue time series in (e): observations after removal of linear temperature (T) and relative humidity (RH) trends from 1948–2018. Red curve: CMIP5 ensemble-mean 50-year low-pass filtered time series (grey areas bound interquartiles of 50-yr low-pass filtered time series among models). Horizontal black lines: Observed mean.

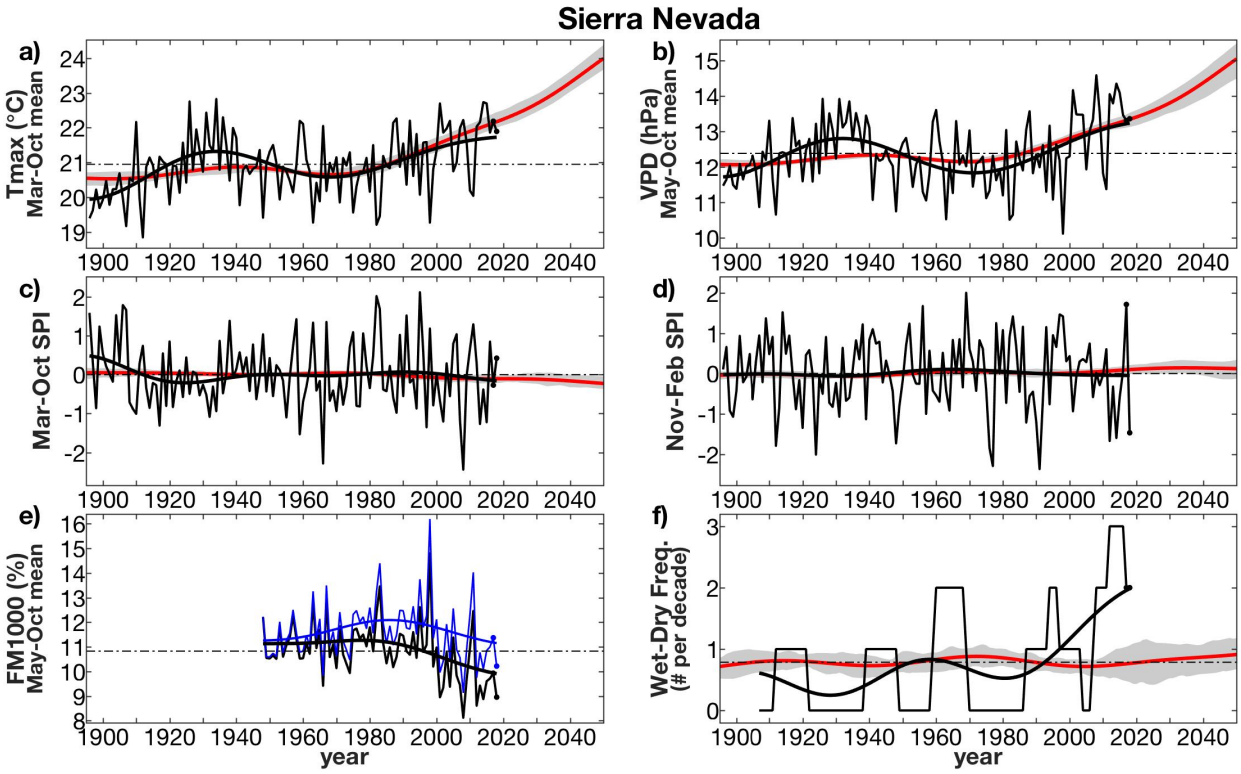

Figure S13. As in Fig. S12 but for the Sierra Nevada region.

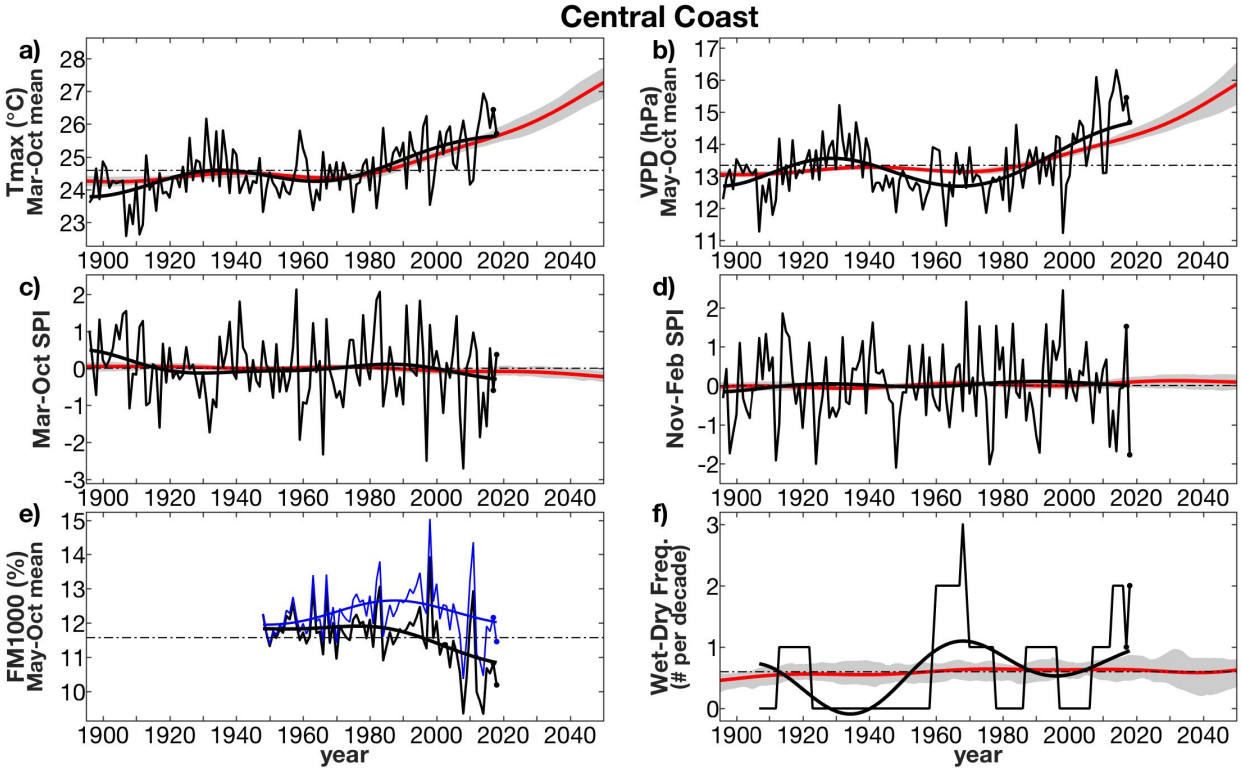

Figure S14. As in Fig. S12 but for the Central Coast region.

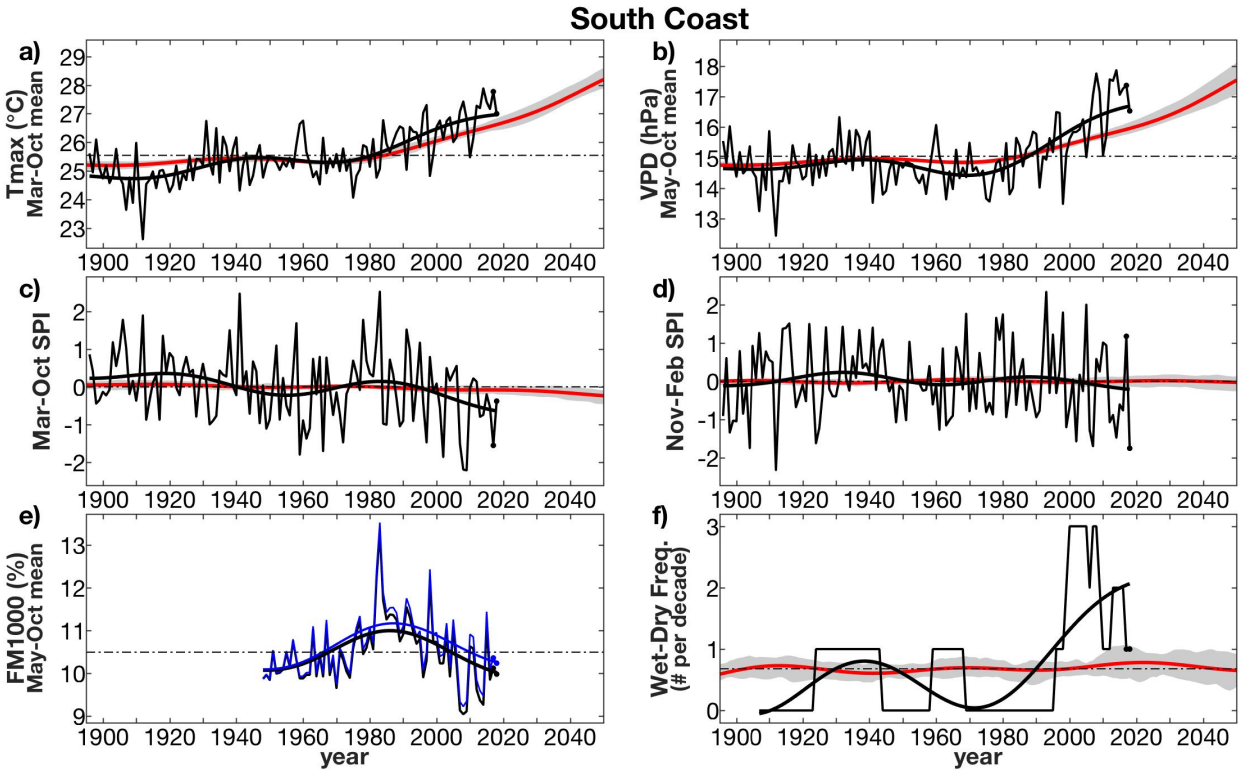

Figure S15. As in Fig. S12 but for the South Coast region.

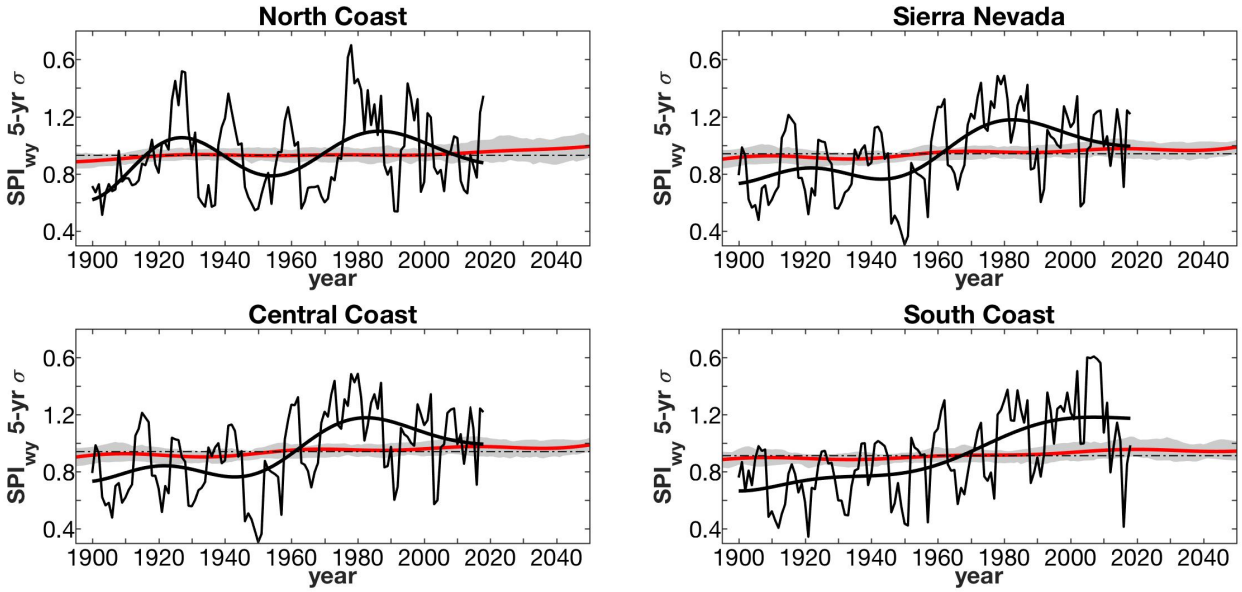

Figure S16. Trends in 5-year running standard deviation (σ) of water-year standardized precipitation index (SPI_{wy}) for each region. Black time series: observations with 50-year low-pass filter. Red: CMIP5 ensemble-mean 50-year low-pass filtered time series (grey areas bound interquartiles among models). Dotted black lines: Observed mean during observed period.

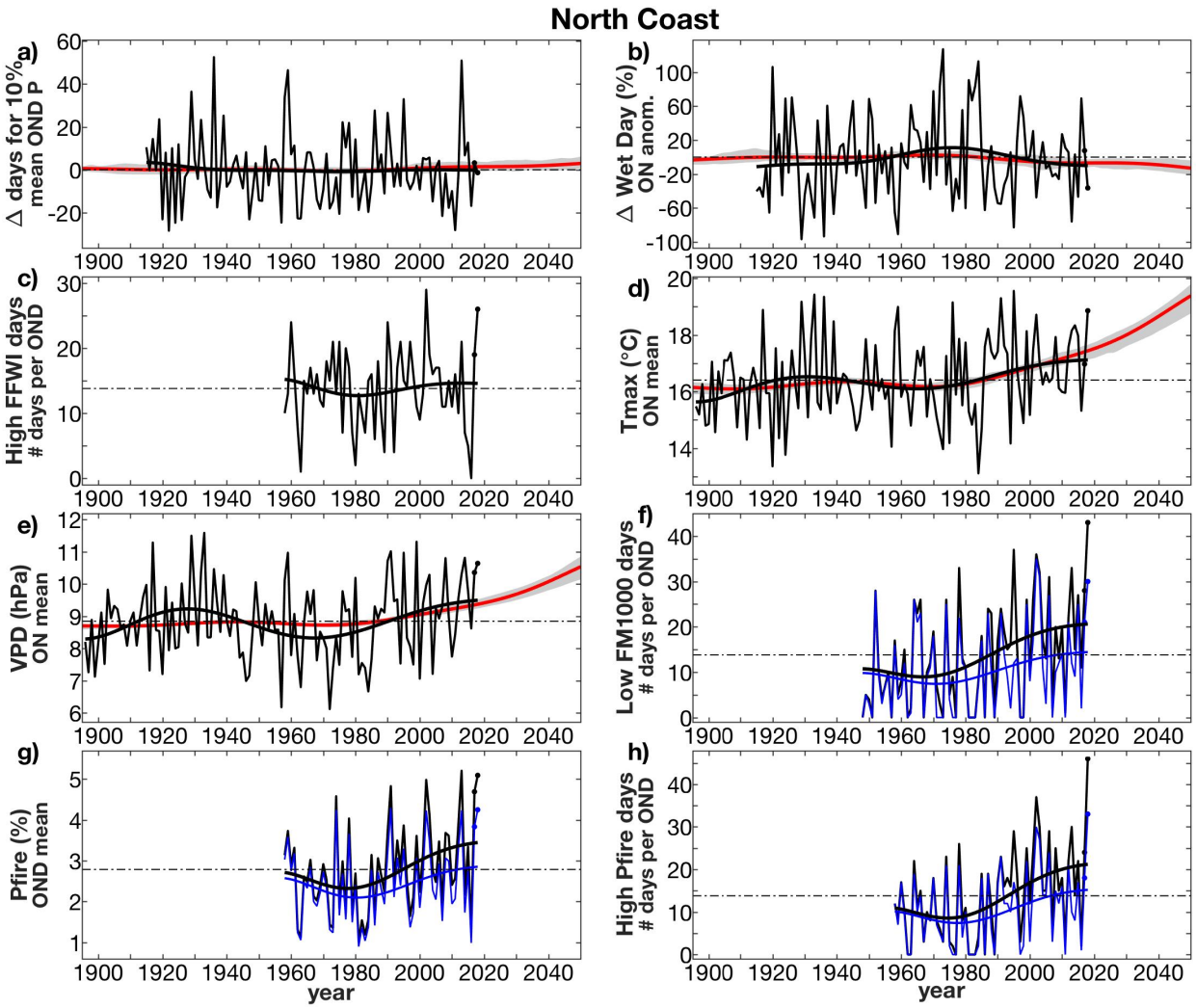

Figure S17. Fall climate trends in the North Coast Region. (a,b) Anomalies in the (a) number of days needed to reach 10% of mean Oct-Dec (OND) precipitation and (b) percent of OND wet days (precipitation total ≥2.54 mm). (c) Number of OND days with Fosberg Fire Weather Index (FFWI) ≥ the 85th percentile. (d,e) Oct-Nov (ON) mean daily maximum temperature (Tmax) and vapor pressure deficit (VPD), respectively. (f) Number of OND days with 1000-hr dead fuel moisture (FM1000) ≤ the 15th percentile. (g,h) OND mean Pfire and number of days with Pfire ≥ the 85th percentile. Pfire: probability of a large (top 5%) OND wildfire, calculated from FM1000 and FFWI. Black time series: observations (2017–2018 indicated with black dots) and (bold curve) 50-year low-pass filter. Blue time series in (f–h): observations after removal of linear temperature (T) and relative humidity (RH) trends from 1948–2018. Red curve: CMIP5 ensemble-mean 50-year low-pass filtered time series (grey areas bound interquartiles of 50-yr low-pass filtered time series among models). Horizontal black lines: Observed mean.

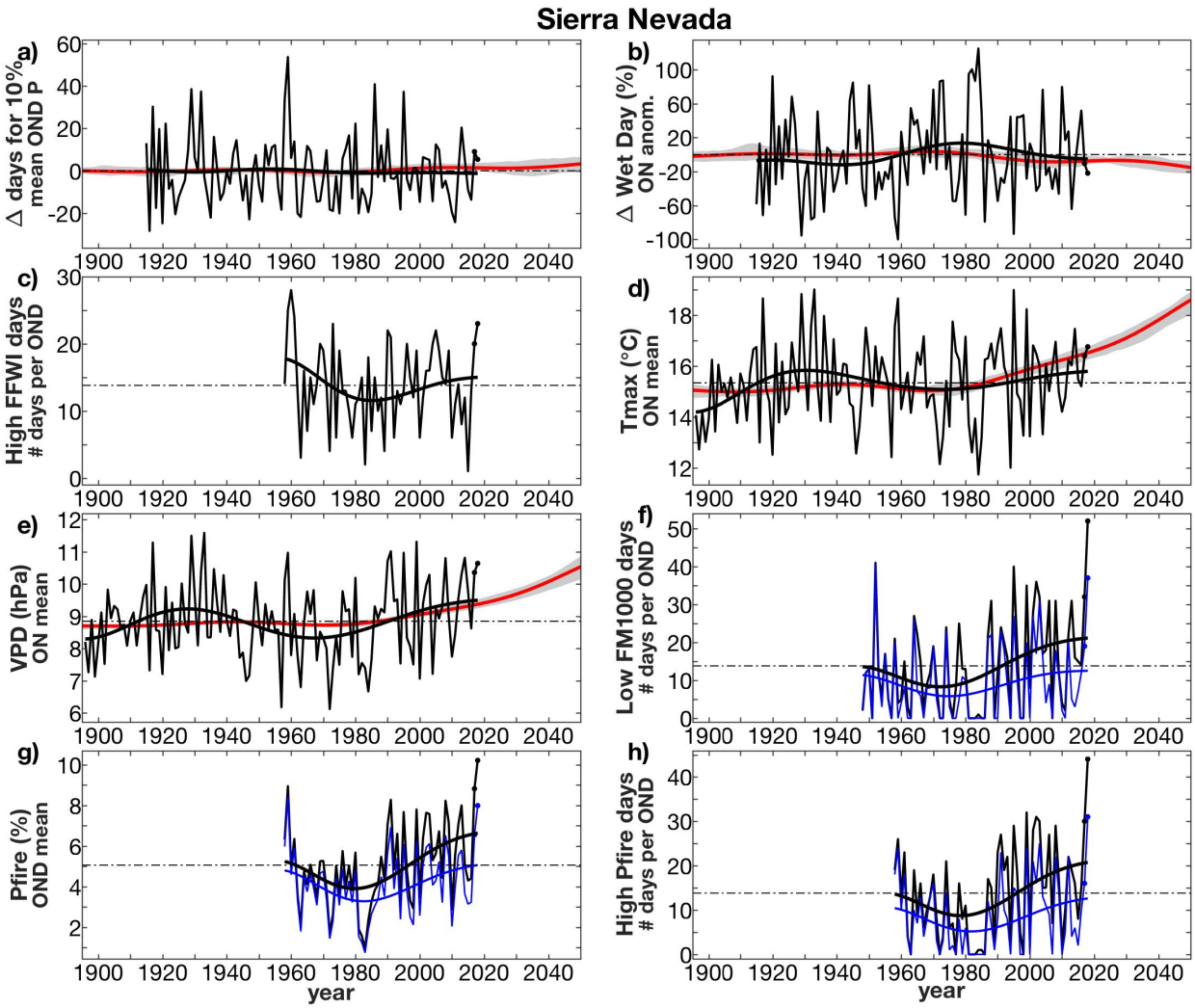

Figure S18. As in Fig. S17 but for the Sierra Nevada region.

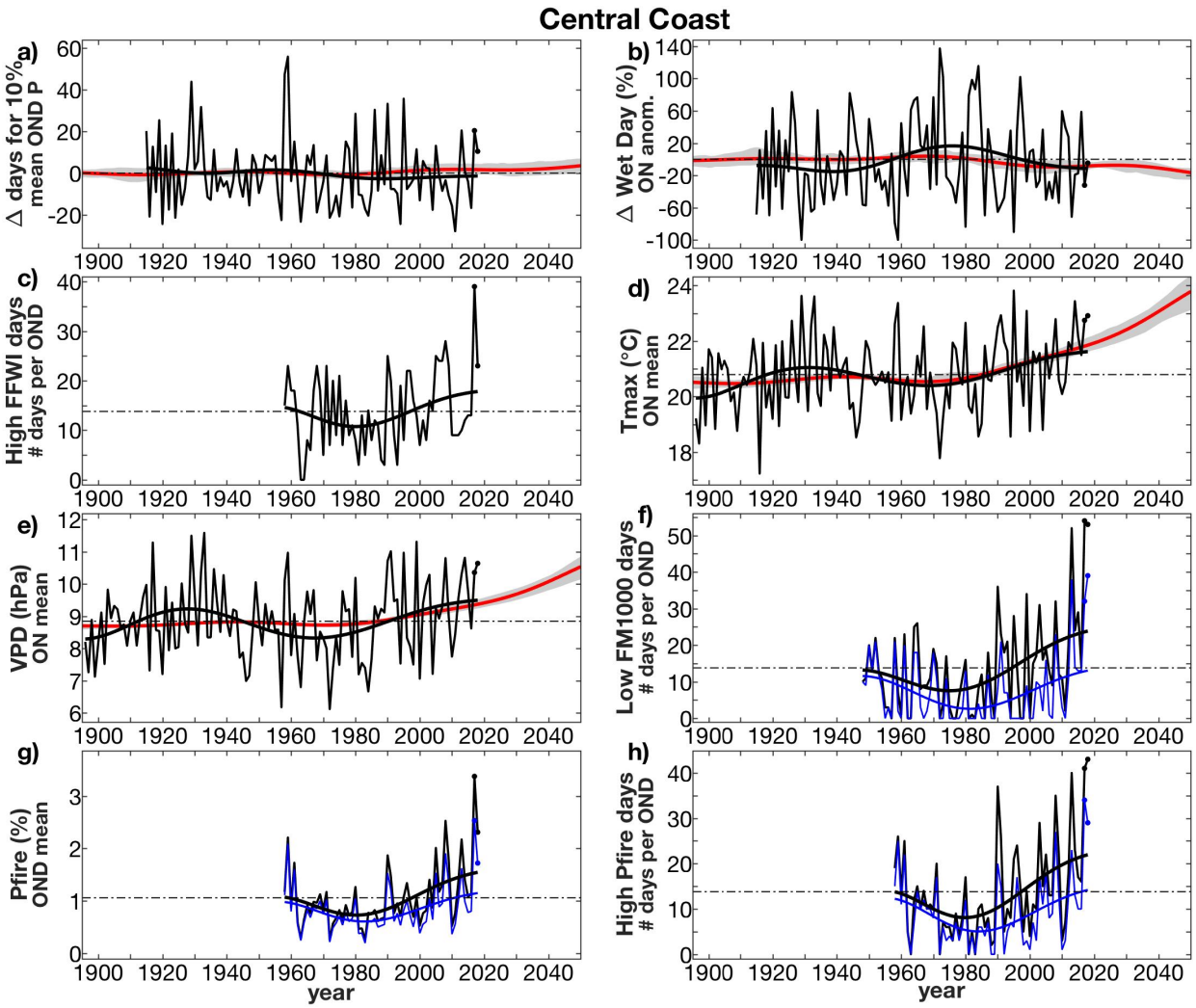

Figure S19. As in Fig. S17 but for the Central Coast region.

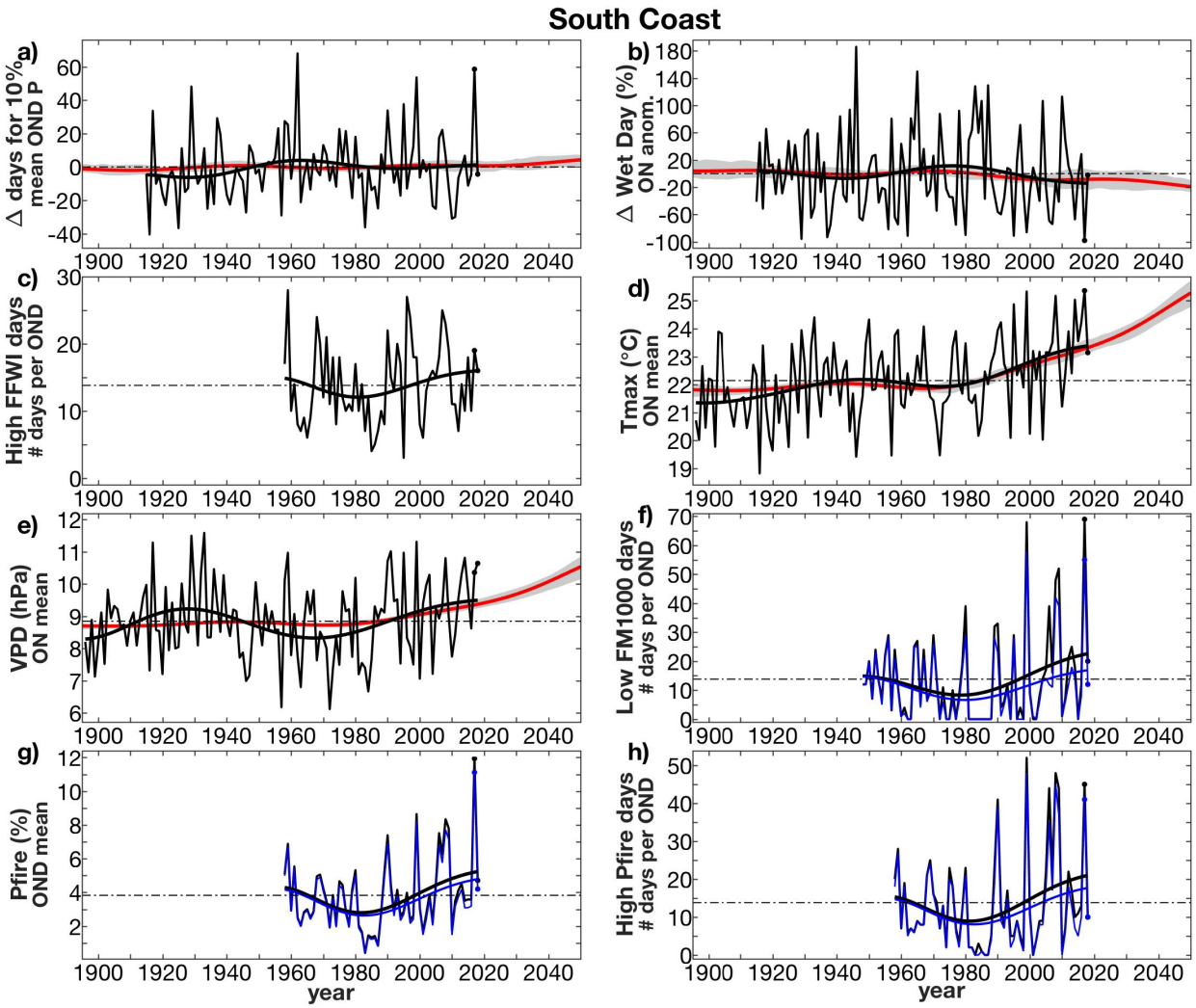

Figure S20. As in Fig. S17 but for the South Coast region.

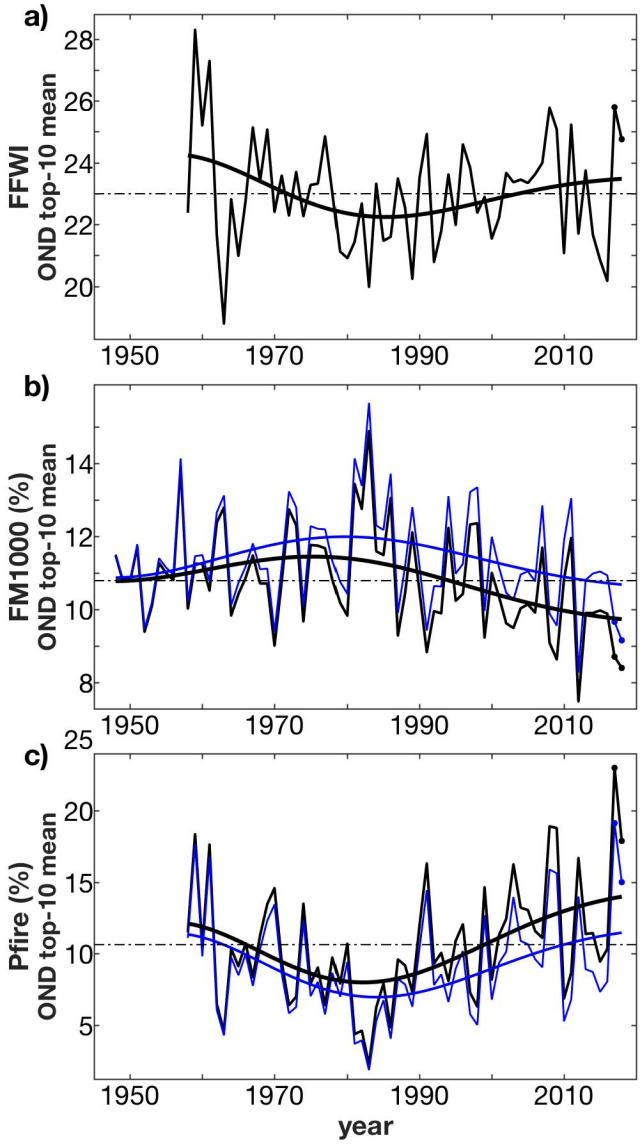

Figure S21. Trends in the mean of the 10 days per Oct-Dec (OND) with the highest fire probability based on (a) Fosberg Fire Weather Index (FFWI), (b) 1000-hour dead fuel moisture (FM1000), and (c) probability of large fall OND wildfire (Pfire). Large wildfires are the largest 5% of OND wildfires in each of the four study regions. Black time series: observations (2017, 2018 indicated with black dots) and (bold curve) 50-year low-pass filter. Blue time series: observations after removal of linear temperature and relative humidity trends from 1948–2018.

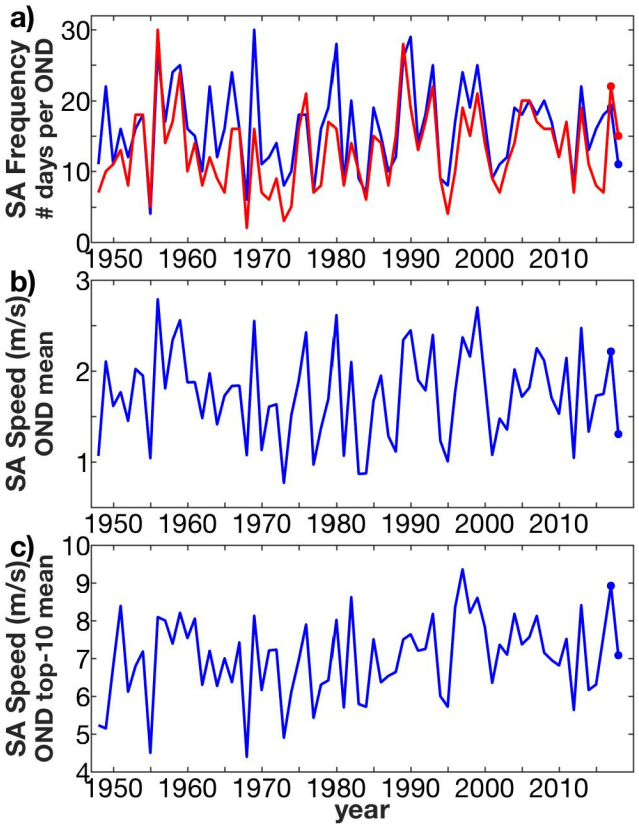

Figure S22. Oct-Dec (OND) Santa Ana (SA) wind indices in southern California based on updated datasets from (blue) Guzman-Morales et al. (2016) and Abatzoglou et al. (2013). The Guzman-Morales dataset is a daily record of mean SA wind speed in the domain of 32.053–35.081 °N, 116.035–118.115 °W. The Abatzoglou et al. record is a daily record of binary SA wind occurrences. (a) Number of Santa Ana (SA) wind days per OND. For Guzman-Morales, SA wind days were classified as days when mean SA wind speed was among the upper 15% of September–March daily SA wind speeds during 1948–2017. (b) Mean daily OND SA wind speed. (c) Mean of the highest daily SA wind speed values each OND. Dots indicate values in 2017 and 2018.